

Prior-preconditioned conjugate gradient method for accelerated Gibbs sampling in ‘large n & large p ’ sparse Bayesian regression

Akihiko Nishimura

Department of Biomathematics, University of California - Los Angeles
and

Marc A. Suchard

Department of Biomathematics, Biostatistics, and Human Genetics,
University of California - Los Angeles

Abstract

In a modern observational study based on healthcare databases, the number of observations and of predictors typically range in the order of $10^5 \sim 10^6$ and of $10^4 \sim 10^5$. Despite the large sample size, data rarely provide sufficient information to reliably estimate such a large number of parameters. Sparse regression techniques provide potential solutions, one notable approach being the Bayesian method based on shrinkage priors. In the “large n & large p ” setting, however, the required posterior computation encounters a bottleneck at repeated sampling from a high-dimensional Gaussian distribution, whose precision matrix Φ is expensive to compute and factorize. In this article, we present a novel algorithm to speed up this bottleneck based on the following observation: we can cheaply generate a random vector \mathbf{b} such that the solution to the linear system $\Phi\boldsymbol{\beta} = \mathbf{b}$ has the desired Gaussian distribution. We can then solve the linear system by the conjugate gradient (CG) algorithm through matrix-vector multiplications by Φ , without ever explicitly inverting Φ . Rapid convergence of CG in this specific context is achieved by the theory of *prior-preconditioning* we develop. We apply our algorithm to a clinically relevant large-scale observational study with $n = 72,489$ patients and $p = 22,175$ clinical covariates, designed to assess the relative risk of adverse events from two alternative blood anti-coagulants. Our algorithm demonstrates an order of magnitude speed-up in the posterior computation.

Keywords: Conjugate gradient, Markov chain Monte Carlo, multivariate Gaussian, numerical linear algebra, sparse matrix, variable selection

1 Introduction

Given an outcome of interest y_i and a large number of features x_{i1}, \dots, x_{ip} for $i = 1, \dots, n$, the goal of sparse regression is to find a small subset of these features that captures the principal relationship between the outcome and features. Such a sparsity assumption is mathematical necessity when p exceeds the sample size n . Even when $n > p$, however, the assumption often remains critical in improving the interpretability and stable estimation of regression coefficients β . This is especially true under the following conditions, either of which reduces the amount of information the data provides on the regression coefficients: 1) the design matrix \mathbf{X} is sparse i.e. only a small fraction of the design matrix contains non-zero entries due to infrequent binary features, and/or 2) the binary outcome \mathbf{y} is rarely observed i.e. $y_i = 0$ for most of i 's. Sparse design matrices are extremely common in modern observational studies based on healthcare databases; while a large number of potential pre-existing conditions and available treatments exist, only a small subset of these applies to each patient (Schuemie et al. 2018b). Rare binary outcomes are also common as many diseases of interest have low incidence rates among the population.

A particular application considered in this manuscript is a comparative study of two blood anti-coagulants *dabigatran* and *warfarin*, using observational data from Truven Health MarketScan Medicare Supplemental and Coordination of Benefits Database. The anti-coagulants help prevent blood clot formation among patients with atrial fibrillation but come with risks of serious side effects. The goal of the study is to quantify which of the two drugs has a lower risk of gastrointestinal bleeding. The data set consists of $n = 72,489$ patients and $p = 22,175$ clinical covariates of potential relevance.

To induce sparsity in the estimate of regression coefficient β , an increasingly common approach is the Bayesian method based on *shrinkage priors*. This class of prior is often represented as a scale-mixture of Gaussians:

$$\beta_j \mid \lambda_j, \tau \sim \mathcal{N}(0, \tau^2 \lambda_j^2), \lambda_j \sim \pi_L(\cdot), \tau \sim \pi_T(\cdot),$$

with unknown *global* and *local scale* parameters τ and λ_j (Carvalho et al. 2010, Polson et al. 2014, Bhattacharya et al. 2015, Bhadra et al. 2017). Compared to more traditional “spike-and-slab” discrete-mixture priors, continuous shrinkage priors are typically more com-

putationally efficient while maintaining highly desirable statistical properties (Bhattacharya et al. 2015, Pal et al. 2014, Datta et al. 2013). Despite the relative computational advantage, however, posterior inference under these priors still faces a serious scalability issue. In the blood anti-coagulant safety study, for instance, it takes nearly 200 hours on a modern high-end commodity desktop to run 10,000 iterations of the current state-of-the-art Gibbs sampler, even with optimized implementation (Section 4).

We focus on sparse logistic regression in this article, but our Gibbs sampler acceleration technique applies whenever the likelihood function can be expressed as a Gaussian mixture. The data augmentation scheme of Polson et al. (2013) makes a posterior under the logistic model amenable to Gibbs sampling as follows. Conditioning on a Polya-Gamma auxiliary parameter $\boldsymbol{\omega}$, the likelihood of a binary outcome \mathbf{y} becomes

$$y'_i | \mathbf{X}, \boldsymbol{\beta}, \boldsymbol{\omega} \sim \mathcal{N}(\mathbf{x}_i^\top \boldsymbol{\beta}, \omega_i^{-1}) \text{ for } y'_i := \omega_i^{-1} (y_i - 1/2). \quad (1.1)$$

Correspondingly, the full conditional distribution of $\boldsymbol{\beta}$ is given by

$$\boldsymbol{\beta} | \boldsymbol{\omega}, \boldsymbol{\lambda}, \tau, \mathbf{y}, \mathbf{X} \sim \mathcal{N}(\boldsymbol{\Phi}^{-1} \mathbf{X}^\top \boldsymbol{\Omega} \mathbf{y}', \boldsymbol{\Phi}^{-1}) \text{ for } \boldsymbol{\Phi} = \mathbf{X}^\top \boldsymbol{\Omega} \mathbf{X} + \tau^{-2} \boldsymbol{\Lambda}^{-2}, \quad (1.2)$$

where $\boldsymbol{\Omega} = \text{diag}(\boldsymbol{\omega})$, a diagonal matrix with entries $\Omega_{ii} = \omega_i$, and $\boldsymbol{\Lambda} = \text{diag}(\boldsymbol{\lambda})$. The main computational bottleneck of the Gibbs sampler is the need to repeatedly sample from high-dimensional Gaussians of the form (1.2). The standard algorithm requires $O(n^2p + p^3)$ operations: $O(n^2p)$ for computing the term $\mathbf{X}^\top \boldsymbol{\Omega} \mathbf{X}$ and $O(p^3)$ for Cholesky factorization of $\boldsymbol{\Phi}$. These operations remain significant burden even with sparsity in \mathbf{X} because computing times of sparse linear algebra operations are dominated not by the number of arithmetic operations but by latency in irregular data access (Dongarra et al. 2016, Duff et al. 2017).

The “large n & large p ” logistic regression problem considered in this article remains unsolved despite the recent computational advances. For $n \ll p$ cases, Bhattacharya et al. (2016) propose an algorithm to sample from (1.2) with only $O(n^2p + n^3)$ operations. Johndrow et al. (2018) reduce the $O(n^2p)$ cost by replacing the matrix $\mathbf{X} \boldsymbol{\Lambda}^2 \mathbf{X}^\top$ with an approximation that can be computed with $O(n^2k)$ operations for $k < p$. These techniques offer no reduction in computational cost for $n > p$ cases, however. Hahn et al. (2018) propose a sampling approach for linear regression based on an extensive pre-processing of the matrix $\mathbf{X}^\top \mathbf{X}$ — a trick limited in scope strictly to Gaussian likelihood models.

Proposed in this article is a novel algorithm to rapidly sample from a high-dimensional Gaussian distribution of the form (1.2) through the conjugate gradient (CG) method, using only a small number of matrix-vector multiplications $\mathbf{v} \rightarrow \Phi \mathbf{v}$. Our algorithm requires no explicit formation of the matrix Φ because we can compute $\Phi \mathbf{v}$ via $\mathbf{v} \rightarrow \mathbf{X} \mathbf{v}$, $\mathbf{w} \rightarrow \mathbf{X}^\top \mathbf{w}$, along with element-wise vector multiplications. This is an important feature not only for computational efficiency but also for memory efficiency when dealing with a large and sparse design matrix \mathbf{X} . The matrix $\mathbf{X}^\top \Omega \mathbf{X}$ and hence Φ typically contain a much larger proportion of non-zero entries than \mathbf{X} , making it much more memory intensive to handle Φ directly. For example, when $p = 10^5$, it would require 74.5 GB of memory to store a $p \times p$ dense matrix Φ in double-precision numbers. On the other hand, our algorithm can exploit a sparsity structure in \mathbf{X} for both computational and memory efficiency.

Practical utility of CG depends critically on effective *preconditioning*, whose purpose is to speed up the algorithm by relating the given linear system to a modified one. Finding an effective preconditioner is a highly problem-specific task and is often viewed as “a combination of art and science” (Saad 2003). Exploiting fundamental features of sparse regression posteriors, we develop the *prior-preconditioning* strategy tailored towards the linear systems in our specific context. We study its theoretical properties and demonstrate its superiority over general-purpose preconditioners in sparse Bayesian regression applications.

The rest of the paper is organized as follows. Section 2 begins by describing how to recast the problem of sampling from the distribution (1.2) as that of solving a linear system $\Phi \boldsymbol{\beta} = \mathbf{b}$. The remainder of the section explains how to apply CG to rapidly solve the linear system, developing necessary theories along the way. In Section 3, we use simulated data to study the effectiveness of our CG sampler in the sparse regression context. Also studied is how the behavior of CG depends on different preconditioning strategies. In Section 4, we apply our algorithm to the blood anti-coagulant safety study, demonstrating an order of magnitude speed-up in the posterior computation. Among the 22,175 predictors, the sparse regression posterior identifies age groups as significant source of treatment effect heterogeneity.

Our CG-accelerated Gibbs sampler is implemented as the *bayesbridge* package available from Python Package Index (pypi.org). The source code is available at a GitHub repository <https://github.com/aki-nishimura/bayes-bridge>.

2 Conjugate gradient sampler

2.1 Generating Gaussian vector as solution of linear system

The standard algorithm for sampling a multivariate-Gaussian requires the Cholesky factorization $\Phi = \mathbf{L}\mathbf{L}^\top$ of its precision (or covariance) matrix (Rue & Held 2005). When the precision matrix Φ has a specific structure as in (1.2), however, it turns out we can recast the problem of sampling from the distribution (1.2) to that of solving a linear system. This in particular obviates the need to compute and factorize Φ .

Proposition 2.1. *The following procedure generates a sample β from the distribution (1.2):*

1. *Generate $\mathbf{b} \sim \mathcal{N}(\mathbf{X}^\top \Omega \mathbf{y}', \Phi)$ by sampling independent Gaussian vectors $\boldsymbol{\eta} \sim \mathcal{N}(\mathbf{0}, \mathbf{I}_n)$ and $\boldsymbol{\delta} \sim \mathcal{N}(\mathbf{0}, \mathbf{I}_p)$ and then setting*

$$\mathbf{b} = \mathbf{X}^\top \Omega \mathbf{y}' + \mathbf{X}^\top \Omega^{1/2} \boldsymbol{\eta} + \tau^{-1} \Lambda^{-1} \boldsymbol{\delta}. \quad (2.3)$$

2. *Solve the following linear system for β :*

$$\Phi \beta = \mathbf{b} \quad \text{where } \Phi = \mathbf{X}^\top \Omega \mathbf{X} + \tau^{-2} \Lambda^{-2}. \quad (2.4)$$

The result follows immediately from basic properties of multivariate Gaussians. The Gaussian vector \mathbf{b} has $\text{Var}(\mathbf{b}) = \Phi$ and is generated with a computational cost negligible compared to computing and factorizing Φ . The solution to (2.4) has the required covariance structure because $\text{Var}(\Phi^{-1} \mathbf{b}) = \Phi^{-1} \text{Var}(\mathbf{b}) (\Phi^{-1})^\top$.

Bhattacharya et al. (2016) proposes a related algorithm which reduces the task of sampling a multivariate Gaussian to solving a $n \times n$ linear system. On the other hand, our algorithm reduces the task to solving a $p \times p$ system, which is smaller in size when $p < n$ and, more importantly, amenable to a fast solution via CG as we will show.

2.2 Iterative method for solving linear system

Proposition 2.1 is useful because solving the linear system (2.4) can be significantly faster than the standard algorithm for sampling a Gaussian vector. We achieve this speed-up by

applying the CG method (Hestenes & Stiefel 1952, Lanczos 1952). CG belongs to a family of *iterative methods* for solving a linear system. Compared to traditional direct methods, iterative methods are more memory efficient and, if the matrix Φ has certain structures (Section 2.3), can be significantly faster.

Iterative methods have found applications in Gaussian process models, where optimizing the hyper parameters of covariance functions requires solving linear systems involving large covariance matrices (Gibbs & MacKay 1996). Significant research has gone into how best to apply iterative methods in this specific context; see Stein et al. (2012), Sun & Stein (2016), and Stroud et al. (2017) for example. Outside the Gaussian process literature, Zhou & Guan (2017) use an iterative method to address the bottleneck of having to solve large linear systems when computing Bayes factors in a model selection problem.

A novel feature of our work is the use of CG as a computational tool for Monte Carlo simulation. A related work is Zhang et al. (2018), brought to our attention while we were preparing the first draft of our manuscript. They use the same idea as in Proposition 2.1 to generate a posterior sample from a Gaussian process model. However, they fail to investigate when and how CG delivers practical computational gains. Our work is distinguished by the development — supported by both theoretical analysis and systematic empirical evaluations — of a novel preconditioning technique tailored toward sparse Bayesian regression problems (Section 2.4 and 2.5). In the process, we also compile a summary of the most practically useful linear algebra results scattered across the literature (Appendix B), facilitating potential applications of CG to a broader range of statistical problems.

The CG method solves a linear system $\Phi\beta = \mathbf{b}$ involving a positive definite matrix Φ as follows. Given an initial guess β_0 , which may be taken as $\beta_0 = \mathbf{0}$ for example, CG generates a sequence $\{\beta_k\}_{k=1,2,\dots}$ of increasingly accurate approximations to the solution. The convergence of the CG iterates β_k 's is intimately tied to the *Krylov subspace*

$$\mathcal{K}(\Phi, \mathbf{r}_0, k) = \text{span} \{ \mathbf{r}_0, \Phi\mathbf{r}_0, \dots, \Phi^{k-1}\mathbf{r}_0 \},$$

generated from the initial residual $\mathbf{r}_0 = \Phi\beta_0 - \mathbf{b}$. With $\beta_0 + \mathcal{K}(\Phi, \mathbf{r}_0, k)$ denoting an affine space $\{\beta_0 + \mathbf{v} : \mathbf{v} \in \mathcal{K}(\Phi, \mathbf{r}_0, k)\}$, the approximate solution β_k satisfies the following

optimality property in terms of a weighted l^2 norm:

$$\beta_k = \operatorname{argmin} \{ \|\beta' - \beta\|_{\Phi} : \beta' \in \beta_0 + \mathcal{K}(\Phi, \mathbf{r}_0, k) \} \quad \text{where } \|\mathbf{r}\|_{\Phi}^2 := \mathbf{r}^\top \Phi \mathbf{r}. \quad (2.5)$$

The norm $\|\cdot\|_{\Phi}$ is often referred to as the Φ -norm. The optimality property (2.5) in particular implies that CG yields the exact solution after p iterations. The main computational cost of each update $\beta_k \rightarrow \beta_{k+1}$ is a matrix-vector operation $\mathbf{v} \rightarrow \Phi \mathbf{v}$. Consequently, the required number of arithmetic operations to run p iterations of the CG update is comparable to that of a direct linear algebra method. For a typical precision matrix Φ in the conditional distribution (1.2), however, we can induce rapid convergence of CG through the preconditioning strategy described in the next section. In our numerical results, we indeed find that the distribution of β_k even for $k \ll p$ is indistinguishable from (1.2) for all practical purposes.

2.3 Convergence of CG and its relation to eigenvalue distribution

The iterative solution $\{\beta_k\}_{k=0,1,2,\dots}$ often displays slow convergence when CG is directly applied to a given linear system. Section 2.4 covers the topic of how to induce more rapid CG convergence for the system (2.4). In preparation, here we describe how the convergence behavior of CG is related to the structure of the positive definite matrix Φ .

CG convergence behavior is partially explained by the following well-known error bound in terms of the *condition number* $\kappa(\Phi)$, the ratio of the largest to smallest eigenvalue of Φ .

Theorem 2.2. *Given a positive definite system $\Phi\beta = \mathbf{b}$ and a starting vector β_0 , the k -th CG iterate β_k satisfies the following bound in its Φ -norm distance to the solution β :*

$$\frac{\|\beta_k - \beta\|_{\Phi}}{\|\beta_0 - \beta\|_{\Phi}} \leq 2 \left(\frac{\sqrt{\kappa(\Phi)} - 1}{\sqrt{\kappa(\Phi)} + 1} \right)^k. \quad (2.6)$$

See Trefethen & Bau (1997) for a proof. Theorem 2.2 guarantees fast convergence of the CG iterates when the condition number is small. On the other hand, a large condition number does not always prevent rapid convergence. This is because CG converges quickly also when the eigenvalues of Φ are “clustered.” The following theorem quantifies this phenomenon, albeit in an idealized situation in which Φ has exactly $k < p$ distinct eigenvalues.

Theorem 2.3. *If the positive definite matrix Φ has only $k + 1$ distinct eigenvalues, then CG yields an exact solution within $k + 1$ iterations. In particular, the result holds if Φ is a rank- k perturbation of an identity i.e. $\Phi = \mathbf{F}\mathbf{F}^\top + \mathbf{I}$ for $\mathbf{F} \in \mathbb{R}^{p \times k}$.*

See Golub & Van Loan (2012) for a proof.

Theorem 2.2 and 2.3 are arguably the most famous results on the convergence property of CG, perhaps because their conclusions are clear-cut and easy to understand. These results, however, fall short of capturing the most important aspects of CG convergence behavior in practice. To address this problem, we bring together the most useful of the known results scattered around the numerical linear algebra literature and summarize them as the following rule of thumb. All the statements below are made mathematically precise in Appendix B.

Rule of Thumb 2.4. *Suppose that the eigenvalues $\nu_p(\Phi) \leq \dots \leq \nu_1(\Phi)$ of Φ are clustered in the interval $[\nu_{p-s}, \nu_r]$ except for a small fraction of them. Then CG effectively “removes” the outlying eigenvalues exponentially quickly. Its convergence rate subsequently accelerates as if the condition number in Eq 2.6 is replaced by the effective value ν_r/ν_{p-s} . The r largest eigenvalues are removed within r iterations, while the same number of smallest eigenvalues tends to delay convergence longer.*

2.4 Preconditioning linear system to accelerate CG convergence

A *preconditioner* is a positive definite matrix \mathbf{M} chosen so that the *preconditioned system*

$$\tilde{\Phi}\tilde{\beta} = \tilde{\mathbf{b}} \quad \text{for } \tilde{\Phi} = \mathbf{M}^{-1/2}\Phi\mathbf{M}^{-1/2} \text{ and } \tilde{\mathbf{b}} = \mathbf{M}^{-1/2}\mathbf{b} \quad (2.7)$$

leads to faster convergence of the CG iterates. In practice, the algorithm can be implemented so that only the operation $\mathbf{v} \rightarrow \mathbf{M}^{-1}\mathbf{v}$, and not $\mathbf{M}^{-1/2}$, is required to solve the preconditioned system (2.7) via CG (Golub & Van Loan 2012). This *preconditioned CG* algorithm still returns a solution $\beta_k = \mathbf{M}^{-1/2}\tilde{\beta}_k$ in terms of the original system.

In light of Rule of Thumb 2.4, an effective preconditioner should modify the eigenvalue structure of Φ so that the preconditioned matrix $\tilde{\Phi}$ has more tightly clustered eigenvalues except for a small number of outlying ones. Larger outlying eigenvalues are preferable over

smaller ones, as smaller ones cause a more significant delay in CG convergence. Additionally, a choice of a preconditioner must take into consideration 1) the one-time cost of computing the preconditioner \mathbf{M} and 2) the cost of operation $\mathbf{v} \rightarrow \mathbf{M}^{-1}\mathbf{v}$ during each CG iteration.

In the contexts of sparse Bayesian regression, the linear system (2.4) admits a deceptively simple yet highly effective preconditioner. As it turns out, the choice

$$\mathbf{M} = \tau^{-2}\mathbf{\Lambda}^{-2}$$

yields a modified system (2.7) with an eigenvalue structure ideally suited to CG. With a slight abuse of terminology, we call it the *prior preconditioner* since it corresponds to the precision of $\boldsymbol{\beta} | \tau, \boldsymbol{\lambda}, \boldsymbol{\omega} (\stackrel{d}{=} \boldsymbol{\beta} | \tau, \boldsymbol{\lambda})$ before observing \mathbf{y} and \mathbf{X} . Most existing preconditioners require explicit access to the elements of $\boldsymbol{\Phi}$ for their constructions (Golub & Van Loan 2012) and are thus useless when computing $\boldsymbol{\Phi}$ itself is a bottleneck. The Jacobi preconditioner $\mathbf{M} = \text{diag}(\Phi_{11}, \dots, \Phi_{pp})$, known as one of the most effective for $\boldsymbol{\Phi}$ with large diagonals, is arguably the only reasonable alternative. Our numerical results clearly show superior performances of the prior preconditioner, however (Section 3.3 and 4.4).

Noting that the prior-preconditioned matrix is given by

$$\tilde{\boldsymbol{\Phi}} = \tau^2\mathbf{\Lambda}\mathbf{X}^\top\boldsymbol{\Omega}\mathbf{X}\mathbf{\Lambda} + \mathbf{I}_p, \tag{2.8}$$

we can heuristically motivate the preconditioner as follows. When employing the shrinkage prior, we expect posterior draws of $\tau\boldsymbol{\lambda}$ to satisfy $\tau\lambda_j \approx 0$ except for a relatively small subset $\{j_1, \dots, j_k\}$ of $j = 1, \dots, p$. The (i, j) -th entry of the matrix $\tau^2\mathbf{\Lambda}\mathbf{X}^\top\boldsymbol{\Omega}\mathbf{X}\mathbf{\Lambda}$ is given by

$$(\tau^2\mathbf{\Lambda}\mathbf{X}^\top\boldsymbol{\Omega}\mathbf{X}\mathbf{\Lambda})_{i,j} = (\tau\lambda_i)(\tau\lambda_j) (\mathbf{X}^\top\boldsymbol{\Omega}\mathbf{X})_{ij},$$

which is small when either $\tau\lambda_i \approx 0$ or $\tau\lambda_j \approx 0$. Hence the entries of $\tau^2\mathbf{\Lambda}\mathbf{X}^\top\boldsymbol{\Omega}\mathbf{X}\mathbf{\Lambda}$ are small away from the $k \times k$ block corresponding to the indices $\{j_1, \dots, j_k\}$. In general, smaller entries of a matrix have less contributions to the eigenvalue structures of the entire matrix (Golub & Van Loan 2012). This means that the prior-preconditioned matrix (2.8) can be thought of as a perturbation of the identity with a matrix of approximate low-rank structure.¹ As

¹It is too naive, however, to deduce that we obtain a good approximation to $\tilde{\boldsymbol{\Phi}}$ by zeroing out $\tau\lambda_j$'s below some threshold. We show in Supplement Section S6 that such approximation is typically of a poor quality.

such, $\tilde{\Phi}$ can be expected to have eigenvalues clustered around 1, except for a small number of larger ones. Supplement Section S1 provides an alternative, and potentially more widely applicable, motivation for the prior-preconditioner based on expected behavior of a posterior under a strongly informative prior.

2.5 Theory of prior-preconditioning and role of posterior sparsity

We now formally quantify the eigenvalue structure of the matrix (2.8).

Theorem 2.5. *Let $\lambda_{(k)} = \lambda_{j_k}$ denote the k -th largest element of $\{\lambda_1, \dots, \lambda_p\}$. The eigenvalues of the prior-preconditioned matrix (2.8) satisfies*

$$1 \leq \nu_k(\tilde{\Phi}) \leq 1 + \tau^2 \lambda_{(k)}^2 \nu_1(\mathbf{X}^\top \Omega \mathbf{X})$$

for $k = 1, \dots, p$. In fact, the following more general bounds hold. Let $\mathbf{A}_{(-k)}$ denote the $(p-k) \times (p-k)$ submatrix of a given matrix \mathbf{A} corresponding to the row and column indices j_{k+1}, \dots, j_p . With this notation, we have

$$1 \leq \nu_{k+\ell}(\tilde{\Phi}) \leq 1 + \tau^2 \lambda_{(k)}^2 \nu_{\ell+1}((\mathbf{X}^\top \Omega \mathbf{X})_{(-k)}) \leq 1 + \tau^2 \lambda_{(k)}^2 \nu_{\ell+1}(\mathbf{X}^\top \Omega \mathbf{X}) \quad (2.9)$$

for any $k \geq 1$ and $\ell \geq 0$ such that $1 \leq k + \ell \leq p$.

Theorem 2.5 guarantees tight clustering of the eigenvalues of the prior-preconditioned matrix — and hence rapid convergence of CG — when most of $\tau \lambda_j$'s are close to zero. Through its dependence on $\nu_\ell(\mathbf{X}^\top \Omega \mathbf{X})$, the bound (2.9) further indicates rapid CG convergence when the eigenvalues of $\mathbf{X}^\top \Omega \mathbf{X}$ decays quickly. We can also relate the prior-preconditioned CG approximation error directly to the decay rate in $\tau \lambda_{(k)}$'s:

Theorem 2.6. *The prior-preconditioned CG applied to (2.4) yields iterates satisfying the following bound for any $m, m' \geq 0$:*

$$\frac{\|\beta_{m+m'} - \beta\|_{\tilde{\Phi}}}{\|\beta_0 - \beta\|_{\tilde{\Phi}}} \leq 2 \left(\frac{\tilde{\kappa}_m^{1/2} - 1}{\tilde{\kappa}_m^{1/2} + 1} \right)^{m'} \quad \text{where } \tilde{\kappa}_m = 1 + \min_{k+\ell=m} \tau^2 \lambda_{(k+1)}^2 \nu_{\ell+1}((\mathbf{X}^\top \Omega \mathbf{X})_{(-k)}). \quad (2.10)$$

See Appendix A for proofs of Theorem 2.5 and 2.6.

To illustrate the implication of Theorem 2.6 in concrete terms, suppose that a posterior draw $\tau, \boldsymbol{\lambda}, \boldsymbol{\omega}$ satisfies $\tau^2 \lambda_{(m+1)}^2 \nu_1(\mathbf{X}^\top \boldsymbol{\Omega} \mathbf{X}) \leq 100$ for some m . In this case, we have $\log_{10} (\tilde{\kappa}_m^{1/2} - 1) / (\tilde{\kappa}_m^{1/2} + 1) \leq -0.086$. So the bound of Theorem 2.6 implies

$$\frac{\|\boldsymbol{\beta}_{m+m'} - \boldsymbol{\beta}\|_{\Phi}}{\|\boldsymbol{\beta}_0 - \boldsymbol{\beta}\|_{\Phi}} \leq 2 \cdot 10^{-0.086m'}.$$

After $m + 100$ iterations, the CG approximation error in the Φ -norm is guaranteed to be reduced by a factor of $2 \cdot 10^{-8.6} \approx 10^{-8.3}$ relative to the initial error.

We have so far stated our theoretical results in purely linear algebraic languages. We now summarize our discussions in a more statistical language, providing a practical guideline on the CG sampler performance in the sparse regression context.

Rule of Thumb 2.7. *The prior-preconditioned CG applied to the linear system (2.4) converges rapidly when the posterior of $\boldsymbol{\beta}$ concentrates on sparse vectors. As the sparsity of $\boldsymbol{\beta}$ increases, the convergence rate of the CG sampler also increases.*

The statements above are born out by illustrative examples of Section 3 using synthetic sparse regression posteriors. As we have seen, the statements can be made more precise in terms of the decay rate in the ordered statistics $\tau \lambda_{(k)}$ of a posterior sample $\tau \boldsymbol{\lambda}$ (Rule of Thumb 2.4, Theorem 2.5, and Theorem 2.6).

2.6 Practical details on deploying CG for sparse regression

While prior preconditioning is undoubtedly the most essential ingredient, there remain a few more important details in applying the CG sampler to sparse regression posterior computation. These are 1) a choice of the initial CG vector $\boldsymbol{\beta}_0$, 2) a termination criteria for CG, and 3) handling of regression coefficients with uninformative priors. We discuss them briefly here and defer more thorough discussions to Supplement Section S2.

A choice of the initial vector has little effect on the eventual exponential convergence rate of CG and, while not to be neglected, is nowhere as consequential as that of the preconditioner (Meurant 2006). In fact, we find that any reasonable choice works fine in our numerical results (Section S2.1). In its typical applications, CG is terminated when the ℓ^2 -norm of the residual $\mathbf{r}_k = \Phi \boldsymbol{\beta}_k - \mathbf{b}$ falls below some prespecified threshold. Utility of

$\|\mathbf{r}_k\|$ as an error metric is dubious for the purpose of the CG sampler, however. We instead propose the prior-preconditioned residual $\tilde{\mathbf{r}}_k = \tilde{\Phi}\tilde{\beta}_k - \tilde{\mathbf{b}}$ as an alternative, more tailored and interpretable for our purpose (Section S2.2). When preconditioning CG, regression coefficients with uninformative priors, such as the intercept, must be handled differently from those under shrinkage. We can accommodate such coefficients by augmenting the prior-preconditioner with another diagonal matrix. We analyze the eigenvalues of the resulting preconditioned matrix and show that the convergence rate remains fast and is robust to the precise choice of the diagonal matrix (Section S2.3).

3 Simulation study of CG sampler performance

We study the CG sampler performance when applied to actual posterior conditional distributions of the form (1.2). We simulate data with varying numbers of non-zero coefficients and confirm how sparsity in regression coefficients translates into faster CG convergence as predicted by Theorem 2.5 and Rule of Thumb 2.7. We also illustrate how the convergence rates are affected by different preconditioning strategies and by corresponding eigenvalue distributions of the preconditioned matrices.

3.1 Choice of shrinkage prior: Bayesian bridge

Among the existing global-local shrinkage priors, in this article we adopt the Bayesian bridge prior of Polson et al. (2014) as the corresponding Gibbs sampler allows for collapsed updates of τ to improve mixing (Polson et al. 2014). The Bayesian bridge Gibbs sampler is in fact uniformly ergodic when the prior tails are properly modified (Nishimura & Suchard 2019).

Under the Bayesian bridge, the local scale λ_j 's are given a prior $\pi(\lambda_j) \propto \lambda_j^{-2} \pi_{\text{st}}(\lambda_j^{-2}/2)$ where $\pi_{\text{st}}(\cdot)$ is an alpha-stable distribution with index of stability $\alpha/2$. The corresponding prior on $\beta_j | \tau$, when λ_j is marginalized out, is

$$\pi(\beta_j | \tau) \propto \tau^{-1} \exp(-|\beta_j/\tau|^\alpha).$$

The distribution of $\beta_j | \tau$ becomes “spikier” as $\alpha \rightarrow 0$, placing greater mass around 0 while inducing heavier tails. In typical applications, the data favors the values $\alpha < 1$ but identifies

α only very weakly (Polson et al. 2014), so in this article we simply fix $\alpha = 1/2$ except when a smaller value seems warranted; see Section 4.3.

3.2 Experimental set-up

We generate synthetic data of sample size $n = 25,000$ with the number of predictors $p = 10,000$. In constructing a design matrix \mathbf{X} , we emulate a model from factor analysis (Jolliffe 2002). We first sample a set of $m = 99$ orthonormal vectors $\mathbf{u}_1, \dots, \mathbf{u}_m \in \mathbb{R}^p$ uniformly from a Stiefel manifold. We then set the predictor \mathbf{x}_i for the i -th observation as

$$\mathbf{x}_i = \sum_{\ell=1}^{99} f_{i,\ell} \mathbf{u}_\ell + \boldsymbol{\epsilon}_i \quad \text{for } f_{i,\ell} \sim \mathcal{N}(0, (100 - \ell)^2) \quad \text{and } \boldsymbol{\epsilon}_i \sim \mathcal{N}(\mathbf{0}, \mathbf{I}_p).$$

This is equivalent to sampling $\mathbf{x}_i \sim \mathcal{N}(\mathbf{0}, \mathbf{U} \mathbf{D} \mathbf{U}^\top)$ for a diagonal matrix \mathbf{D} with $\sqrt{D_{\ell\ell}} = \max\{100 - \ell, 1\}$ and an orthonormal matrix \mathbf{U} sampled uniformly from the space of orthonormal matrices. We then center and standardize the predictors as is commonly done before applying sparse regression (Hastie et al. 2009).

The above process yields a design matrix \mathbf{X} with moderate correlations among the p predictors — the distribution of pairwise correlations is approximately Gaussian centered around 0 with the standard deviation of 0.13. Based on this design matrix \mathbf{X} , we simulate three different binary outcome vectors by varying the number of non-zero regression coefficients. More specifically, we consider a sparse regression coefficient $\boldsymbol{\beta}_{\text{true}}$ with $\beta_{\text{true},j} = \mathbb{1}\{j \leq K\}$ with varying numbers of signals $K = 10, 20, \text{ and } 50$. In all three scenarios, the binary outcome y_i 's are generated from the logistic model as $y_i | \boldsymbol{\beta}_{\text{true}}, \mathbf{x}_i \sim \text{Bernoulli}(p_i)$ for $\text{logit}(p_i) = \mathbf{x}_i^\top \boldsymbol{\beta}_{\text{true}}$.

For each synthetic data set, we obtain a posterior sample of $\boldsymbol{\omega}, \tau, \boldsymbol{\lambda} | \mathbf{y}, \mathbf{X}$ by running the Polya-Gamma augmented Gibbs sampler with the brute-force direct linear algebra to sample $\boldsymbol{\beta}$ from its conditional distribution (1.2). We confirm the convergence of the Markov chain by examining the traceplot of the posterior log-density of $\boldsymbol{\beta}, \tau | \mathbf{y}, \mathbf{X}$. Having obtained a posterior sample $(\boldsymbol{\omega}, \tau, \boldsymbol{\lambda})$, we sample a vector \mathbf{b} as in (2.3) and apply CG to the linear system (2.4). We compare the CG iterates $\{\boldsymbol{\beta}_k\}_{k \geq 0}$ to the exact solution $\boldsymbol{\beta}_{\text{direct}}$ obtained by solving the same system with the Cholesky-based direct method. We repeat this process for eight random replications of the right-hand vector \mathbf{b} .

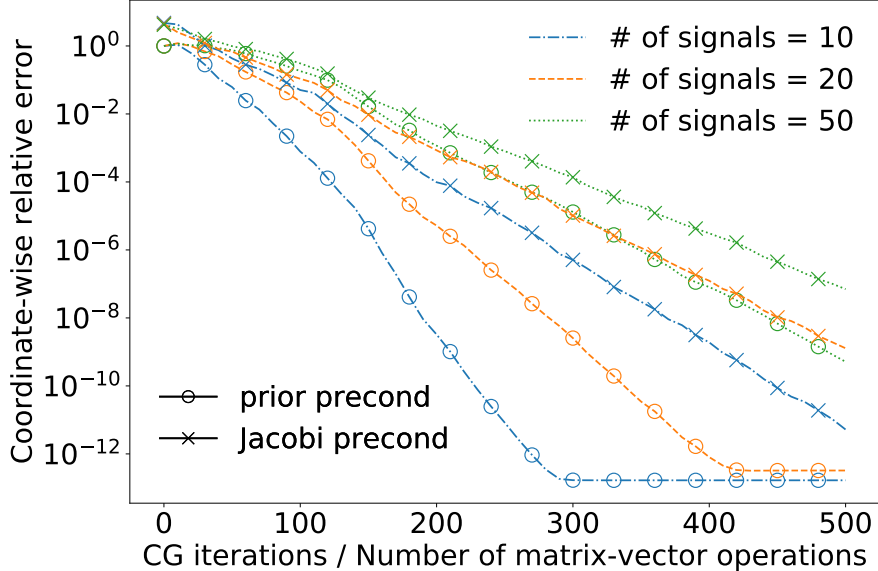


Figure 3.1: Plot of the CG approximation error vs. the number of CG iterations. The CG sampler is applied to synthetic sparse regression posteriors. The different line styles correspond to the different numbers of true signals. The circle and cross markers denote the uses of the prior and Jacobi preconditioners.

3.3 Results: convergence rates, eigenvalues, and sparsity

Figure 3.1 shows the CG approximation error as a function of the number of CG iterations, whose cost is dominated by matrix-vector multiplications $\mathbf{v} \rightarrow \Phi \mathbf{v}$. We characterize the approximation error as the relative error $|(\boldsymbol{\beta}_k - \boldsymbol{\beta}_{\text{direct}})_j / (\boldsymbol{\beta}_{\text{direct}})_j|$ averaged across all the coefficients. Each line on the plot shows the geometric average of this error metric over the eight random replications of \mathbf{b} . The CG convergence behavior observed here remains qualitatively similar regardless of the error metric choice and varies little across the different right-hand vectors (Supplement Section S3).

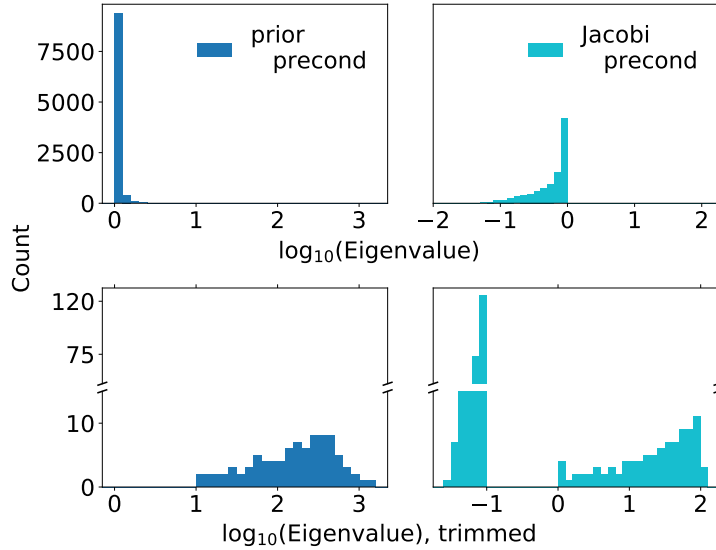
We first focus on the approximation errors under the prior preconditioner, indicated by the lines with circles. After $k \ll p = 10,000$ matrix-vector operations, the distance between $\boldsymbol{\beta}_k$ and $\boldsymbol{\beta}_{\text{direct}}$ is already orders of magnitudes smaller than typical Monte Carlo errors. With additional CG iterations, the distance reaches the machine precision level; notice the eventual “plateaus” achieved under the prior preconditioner in the $K = 10$ and $K = 20$ cases.

Figure 3.1 also shows the approximation errors under the Jacobi preconditioner $\mathbf{M} =$

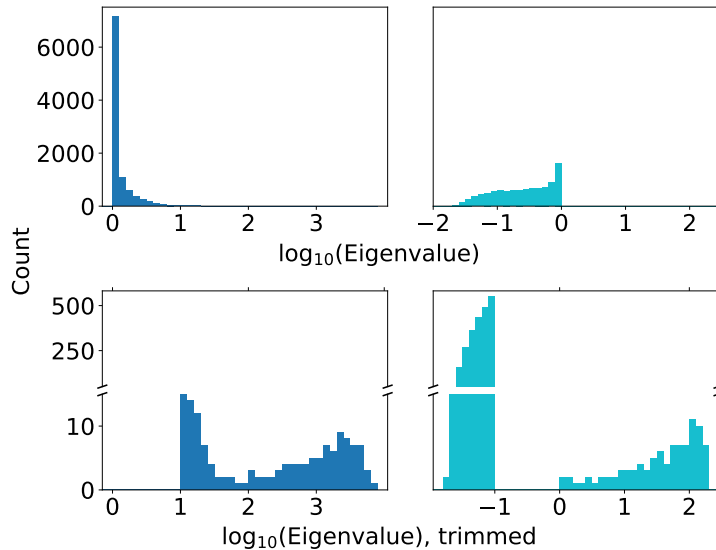
$\text{diag}(\Phi_{11}, \dots, \Phi_{pp})$ which, as discussed in Section 2.4, is the only reasonable alternative when using the CG sampler for the applications considered in this article. The prior preconditioner is clearly superior, with the difference in convergence speed more pronounced when true regression coefficients are sparser. Studying the eigenvalue distributions of the respective preconditioned matrices provides further insight into the observed convergence behaviors. Figure 3.3 (a) & (b) show the eigenvalue distributions of the preconditioned matrices based on a posterior sample from the synthetic data with $K = 10$. The trimmed version of the histograms highlight the tails of the distributions. The prior preconditioner induces the distribution with a tight cluster around 1 (or 0 in the \log_{10} scale) with a relatively small number of large ones, confirming the theory developed in Section 2.5. On the other hand, the Jacobi preconditioner induces a more spread-out distribution, problematically introducing quite a few small eigenvalues that delay the CG convergence (Rule of Thumb 2.4).

Finally, we turn our attention to the relationship, as seen in Figure 3.1, between CG convergence rate and sparsity in the underlying true regression coefficients. The convergence is clearly quicker when the true regression coefficients are sparser. To understand this relationship, it is informative to look at the values of $\tau\lambda_j = \text{var}(\beta_j | \tau, \boldsymbol{\lambda})^{1/2}$ drawn from the respective posterior distributions. Figure 3.3 plots the values of $\tau\lambda_j$ for $j = 1, \dots, 250$ corresponding to the first 250 coefficients. We use two different y -scales for $K = 10$ and $K = 50$, shown on the left and right respectively, to facilitate qualitative comparison between the two cases. As expected, the posterior sample from the synthetic data with a larger number of signals has a larger number of $\tau\lambda_j$'s away from zero. These relatively large $\tau\lambda_j$'s contribute to the delayed convergence of CG (Theorem 2.5 and Rule of Thumb 2.4).

A more significant cause of the delay, however, is the fact that the shrinkage prior yields weaker shrinkage on the zero coefficients when there are a larger number of signals. With a close look at Figure 3.3, one can see that $\tau\lambda_1, \dots, \tau\lambda_K$ corresponding to the true signals are not as well separated from the rest of $\tau\lambda_j$'s when $K = 50$. In fact, the histograms on the left of Figure 3.4 shows that the distribution of $\tau\lambda_j$'s for $K = 50$ are shifted toward larger values compared to that for $K = 10$. This is mostly due to the posterior distribution of τ concentrating around a larger value — the value of the posterior sample is $\tau \approx 2.0 \times 10^{-3}$ for the $K = 10$ case while $\tau \approx 6.7 \times 10^{-3}$ for the $K = 50$ case. It is also worth taking a closer look



(a) Based on synthetic data with 10 non-zero coefficients.



(b) Based on synthetic data with 50 non-zero coefficients.

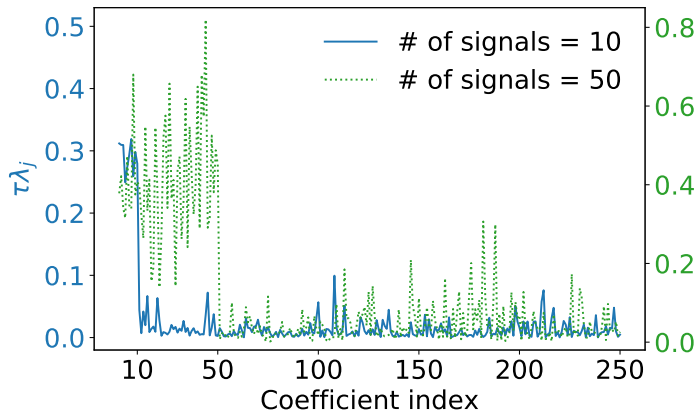


Figure 3.2: Histograms of the eigenvalues of the preconditioned matrices. The eigenvalues under the prior preconditioner are shown on the left and those under the Jacobi on the right. Shown on the lower row are the trimmed versions of the histograms, in which we remove the eigenvalues in the range $[0, 1]$ in the \log_{10} scale for the prior preconditioner and those in the range $[-1, 0]$ for the Jacobi. The y -axes for the trimmed histograms have intermediate values removed to make small counts more visible. The width of the bins are kept constant throughout so that the y -axis values of the bars are proportional to probability densities and thus can be compared meaningfully across the plots.

Figure 3.3: Plot of the posterior samples of $\tau\lambda_j$'s for $j = 1, \dots, 250$. The solid blue line and dashed green line correspond to the data sets simulated with $\beta_{\text{true},j} = 1$ for $j \leq 10$ and for $j \leq 50$ respectively.

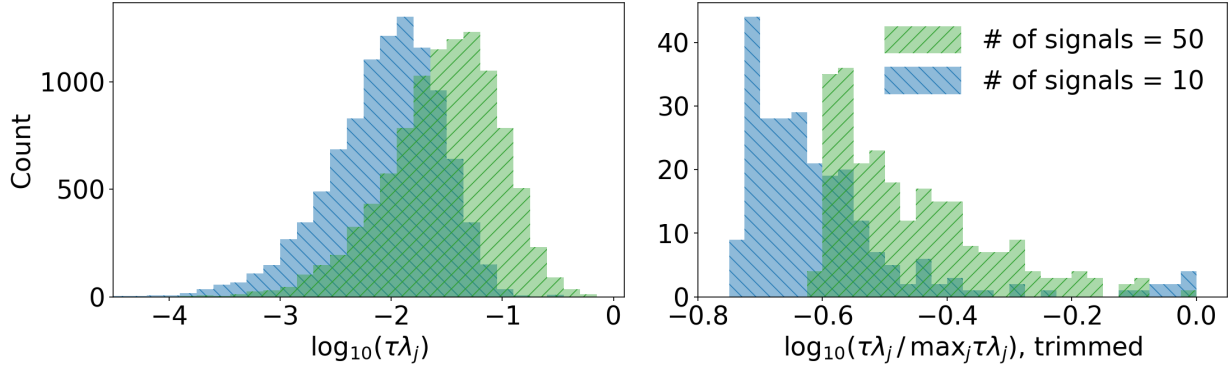


Figure 3.4: Histograms of the posterior samples of $\tau\lambda_j$'s. The two different colors indicate the distinct posteriors with 10 and 50 non-zero regression coefficients. To better expose the relative tail behaviors in the two distributions of $\tau\lambda_j$'s, the histograms on the right take the 250 largest values and plot their magnitudes relative to $\max_j \tau\lambda_j$.

at the tail of the distribution of $\tau\lambda_j$'s. The histograms on the right of Figure 3.4 show the distribution of the 250 largest $\tau\lambda_j$'s. The figure makes it clear that $\tau\lambda_j$'s corresponding to the true signals are much more well separated from the rest when $K = 10$. Overall, the slower decay in the largest values of $\tau\lambda_j$'s results in the eigenvalues of the preconditioned matrices having a less tight cluster around 1; compare the eigenvalue distributions of Figure 3.3.(a) & (b) to those of Figure 3.3.(c) & (d).

4 Application: comparison of alternative treatments

In this section, we demonstrate the magnitude of speed-up delivered by CG-acceleration in modern large-scale applications. We apply sparse Bayesian logistic regression to conduct a comparative study of two blood anti-coagulants *dabigatran* and *warfarin*. The goal of the study is to quantify which of the two drugs have a lower risk of gastrointestinal bleeding. This question has previously been investigated by Graham et al. (2015) and our analysis yields clinical findings consistent with theirs (Section 4.5).

We are particularly interested in sparse Bayesian regression as a tool for the Observational Health Data Sciences and Informatics (OHDSI) collaborative (Hripcsak et al. 2015). We therefore follow the OHDSI protocol in pre-processing of the data as well as in estimating the treatment effect. In particular, sparse regression plays a critical role in eliminating hand-

picking of confounding factors and of subgroups for testing treatment effect heterogeneity; this enables the application of a reproducible and consistent statistical estimation procedure to tens of thousands of observational studies (Schuemie et al. 2018 b,a , Tian et al. 2018).

4.1 Data set

We extract patient-level data from Truven Health MarketScan Medicare Supplemental and Coordination of Benefits Database. In the database, we find $n = 72,489$ patients who became first-time users of either dabigatran or warfarin after diagnosis of atrial fibrillation. Among them, 19,768 are treated with dabigatran and the rest with warfarin. There are $p = 98,118$ predictors, consisting of clinical measurements, pre-existing conditions, as well as prior treatments and administered drugs — all measured before exposure to dabigatran or warfarin. Following the OHDSI protocol, we screen out the predictors observed in less than 0.1% of the cohort. This reduces the number of predictors to $p = 22,175$. The precise definition of the cohort can be found at <http://www.ohdsi.org/web/atlas/#/cohortdefinition/{2978,2979,2981}>.

Each patient is affected by only a small fraction of the potential pre-existing conditions and available treatments. The design matrix \mathbf{X} therefore is sparse, with only 4% of the entries being non-zero. Another noteworthy feature of the data is the low incidence rates of gastrointestinal bleeding; the outcome indicator \mathbf{y} has non-zero entries $y_i = 1$ for only 713 out of 72,489 patients.

4.2 Statistical approach: propensity score stratified regression

To control for covariate imbalances between the dabigatran and warfarin users, we rely on propensity score method in estimating the treatment effect. The procedure involves two logistic models with large numbers of predictors, to deal with which we employ sparse Bayesian regression. We describe the procedure and essential ideas below but refer the readers to Stuart (2010), and the references therein for further details.

Estimation of the treatment effect proceeds in two stages. First, the *propensity score*

$\mathbb{P}(T_i = 1 | \mathbf{x}_i)$ of the treatment assignment to dabigatran is estimated by the logistic model

$$\text{logit}\{\mathbb{P}(T_i = 1 | \mathbf{x}_i)\} = \beta_0 + \mathbf{x}_i^\top \boldsymbol{\beta}. \quad (4.11)$$

While not of direct interest within the propensity score method framework, identifying significant predictors of the score is highly relevant in the OHDSI applications. Many of the databases are too small to fit the models with such large numbers of predictors, but the significant heterogeneity among them makes the joint estimation insensible (Hripcsak et al. 2016). Sparse regression provides a tool to screen out the predictors using the larger databases and use only the selected subset to estimate the scores within the smaller databases.

After fitting the model (4.11), the quantiles of the estimated propensity scores are then used to stratify the population into subpopulations of equal sizes. Following a typical recommendation, we choose the number of strata as $M = 5$. Under suitable assumptions, conditioning on the strata indicator removes most of imbalances in the distributions of the predictors between the treatment ($T_i = 1$) and control ($T_i = -1$) groups. After the stratification, we can proceed to estimate the treatment effect via the logistic model without the main effect from the clinical covariate \mathbf{x}_i (Tian et al. 2014):

$$\text{logit}\{\mathbb{P}(y_i = 1 | \boldsymbol{\alpha}, \boldsymbol{\gamma}, s_i, \mathbf{x}_i)\} = \sum_{m=1}^M \alpha_m \mathbb{1}\{s_i = m\} + (\alpha_0 + \mathbf{x}_i^\top \boldsymbol{\gamma}) T_i, \quad (4.12)$$

where a categorical variable s_i denotes the strata membership of the i -th individual. The quantity $(\alpha_0 + \mathbf{x}^\top \boldsymbol{\gamma})$ represents the treatment effect for a patient with covariate \mathbf{x} , with the feature x_{ij} contributing to the treatment effect heterogeneity when $\gamma_j \neq 0$. The goal of sparse regression here is to identify such nonzero γ_j 's.

4.3 Prior choice and posterior computation

We fit the models (4.11) and (4.12) using the Bayesian bridge shrinkage prior (Section 3.1). For the main treatment and propensity score strata effects, we place weakly informative $\mathcal{N}(0, 1)$ priors. For the global scale parameter, we use an objective prior $\pi(\tau) \propto 1/\tau$ in the model (4.11) (Berger et al. 2009). For the treatment effect model (4.12), due to the low incidence rate in the outcome, we find the above prior choice to provide insufficient separation of significant predictors from the rest. We therefore use the bridge prior with $\alpha = 1/4$ and

weakly informative conjugate prior $\phi = \tau^{-\alpha} \sim \text{Gamma}(\text{shape} = 339.8, \text{rate} = 26.58)$ so that $\log_{10}(\tau)$ has the prior mean of -1.5 and standard deviation of 0.5 .

For posterior computation, we compare two Gibbs samplers that differ only in their methods for drawing β from the conditional distribution (1.2). One sampler uses the proposed CG sampler while the other uses a traditional direct method via Cholesky factorization. Sparse Cholesky methods offer no computational benefit here as the precision matrix, despite the sparsity in the design matrix \mathbf{X} , is almost completely dense (Supplement Section S4). We refer to the respective samplers as the *CG-accelerated* and *direct* Gibbs sampler. The other conditional updates follow the approaches described in Polson et al. (2014).

We implement the Gibbs samplers in Python and run on 2015 iMac with four Intel Core i7 processors. Linear algebra being the computational bottleneck, both samplers benefit from parallelization and we engage all the four CPU's. For the linear algebra operations, we interface our Python code with the Intel Math Kernel Library (MKL) implementations of Basic Linear Algebra Subprograms (BLAS) and sparse BLAS, which proved computationally superior to alternatives in our preliminary benchmarking. Details on how we optimized both Gibbs sampler are described in Supplement Section S4.

We run the Gibbs samplers for 5,500 and 11,000 iterations for the propensity score and treatment effect model, discarding the first 500 and 1,000 as burn-ins. We confirm their convergences by examining the traceplots of the posterior log-density. We estimate the effective sample sizes (ESS) for all the regression coefficients using the R package CODA. The smallest ESSs are found among the coefficients with bimodal posteriors, but their traceplots nonetheless indicate reasonable mixing. We find the minimum and median ESS to be 106.2 and 2484 for the propensity score model, and 86.04 and 2496 for the treatment effect model.

4.4 CG acceleration magnitudes and posterior characteristics

The direct Gibbs sampler requires 106 and 212 hours for the propensity score and treatment effect model. On the other hand, the CG-accelerated sampler finishes in 11.4 and 11.3 hours, yielding **9.3-fold** and **18.8-fold** speed-ups. For both Gibbs samplers, the total computation times are dominated by the conditional updates of β . The magnitudes of CG-acceleration thus are determined by the CG convergence rate at each Gibbs iteration.

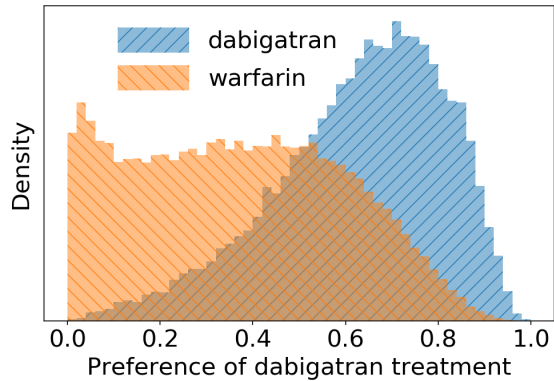


Figure 4.5: Normalized histogram of the estimated preference scores for each group. Preference score transforms raw propensity score to make it a more interpretable measure (Walker et al. 2013).

In agreement with the theory and empirical results of Section 2.5 and 3.3, the variability in the magnitudes of CG-acceleration can be explained by the posterior sparsity structures of the regression coefficients. For the propensity score model, 82 out of the 22,175 regression coefficients have their posterior mean magnitude above 0.1, while 18,187 (82.0%) of the coefficients below 0.01. For the treatment effect model, only 2 of the coefficients have the posterior mean magnitudes above 0.1, while 22,096 (99.6%) below 0.01. We note that the individual posterior samples are much less sparse than the posterior mean. Under the treatment effect model, for example, the number of coefficients with magnitude above 0.1 typically ranges from 265 to 529 while those below 0.01 from 16,172 to 17,632.

For more in-depth analysis of the CG-acceleration mechanism, in Supplement Section S5 we examine the CG sampler behavior at each Gibbs iteration. In particular, we verify that the error metric discussed in Section 2.6 works well in deciding when to terminate the CG iteration. We also confirm that the prior preconditioner continues to outperform the Jacobi in this real data example.

4.5 Clinical conclusions from dabigatran vs. warfarin study

The propensity score model finds substantial differences between the patients treated by dabigatran and warfarin. In particular, patients' covariate characteristics are predictive of the treatment assignments as seen in Figure 4.5. The two most significant predictors are the treatment year and age group. Both predictors have been encoded as binary indicators in the design matrix for simplicity, but the coefficients of categorical and ordinal predictors

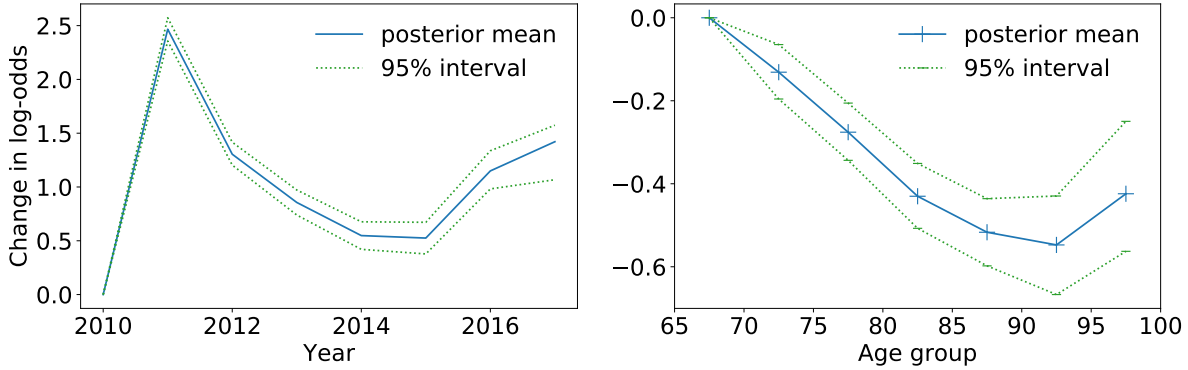
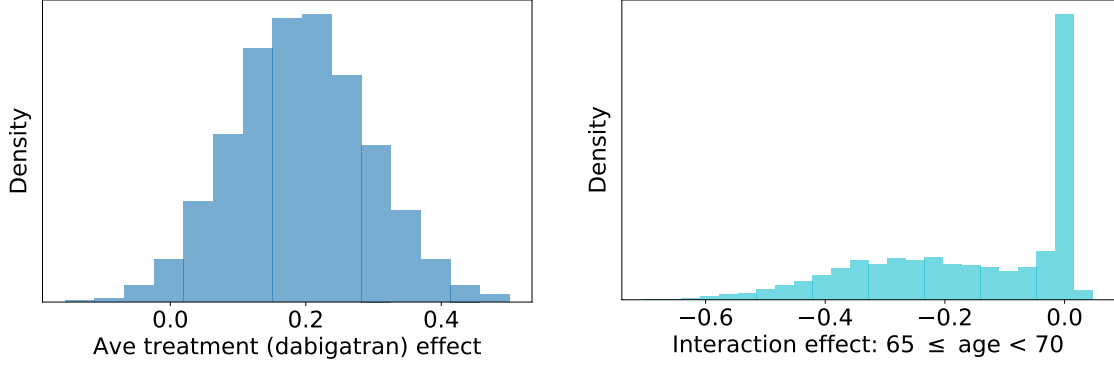


Figure 4.6: Posterior means and 95% credible intervals for the regression coefficients of the treatment year and age group indicators. The age groups are divided into 5-year windows.

could have been estimated with shrinkage priors analogous to Bayesian grouped or fused lasso (Kyung et al. 2010, Xu et al. 2015). The posterior mean and 95% credible intervals of the regression coefficients are shown in Figure 4.6. The figure plots the effect sizes relative to the year 2010 and the age group 65–69; when actually fitting the model, however, we use the most common category as a baseline for categorical variables.

For the treatment effect model, Figure 4.7(a) shows the posterior distribution of the average treatment effect of dabigatran over warfarin. The posterior indicates an evidence for the lower incidence rate of gastrointestinal bleeding under dabigatran treatment, which is consistent with findings of Graham et al. (2015). Remarkably, our sparse regression model identifies substantial interaction between the treatment and age group 65–69, with effect size potentially large enough to offset the average treatment effect. No other age groups exhibit significant interaction with the treatment. The 65–69 age group being the youngest in our Medicare cohort, our finding suggests a possibility that the relative risk of gastrointestinal bleeding only increases in the older patients. In fact, Graham et al. (2015) reports the risks from dabigatran and warfarin to be comparable for women under 75 and men under 85 years old. A potential concern with their results is the lack of explanation on their choices of age thresholds. On the other hand, our subgroup detection approach based on sparse regression avoids an arbitrary selection of subgroups when studying treatment effect heterogeneity.



(a) Average effect of treatment by dabigatran over warfarin on gastrointestinal bleeding. (b) Coefficient of the interaction between treatment and age group 65–69.

Figure 4.7: Posterior distributions from the treatment effect model.

5 Acknowledgment

We thank Yuxi Tian and Martijn Schuemie for their help in wrangling the data set used in Section 4. We also thank Jianfeng Lu and Ilse Ipsen for useful discussions on linear algebra topics. This work is partially supported by National Science Foundation grant DMS 1264153 and National Institutes of Health grant U19 AI135995.

Appendix A Proofs

Before we proceed to proving Theorem 2.5, we first derive Theorem 2.6 as its consequence.

Theorem 2.6. By Theorem B.4, the $(m + m')$ -th CG iterate $\beta_{m+m'}$ satisfies the bound

$$\frac{\|\beta_{m+m'} - \beta\|_{\Phi}}{\|\beta_0 - \beta\|_{\Phi}} \leq 2 \left(\frac{\sqrt{\nu_{m+1}/\nu_p} - 1}{\sqrt{\nu_{m+1}/\nu_p} + 1} \right)^{m'}, \quad (\text{A.13})$$

where ν_j denotes the j -th largest eigenvalue of Φ . By Theorem 2.5, we know that

$$1 \leq \nu_p \leq \nu_{m+1} \leq 1 + \min_{k+\ell=m} \tau^2 \lambda_{(k+1)}^2 \nu_{\ell+1} ((\mathbf{X}^\top \Omega \mathbf{X})_{(-k)}) = \tilde{\kappa}_m$$

and hence that $\nu_{m+1}/\nu_p \leq \tilde{\kappa}_m$. Since the function $\kappa \rightarrow (\sqrt{\kappa} - 1)/(\sqrt{\kappa} + 1)$ is increasing in κ , we can upper bound the right-hand side of (A.13) in terms of $\tilde{\kappa}_m$, yielding the desired inequality (2.10). \square

Theorem 2.5. We prove the more general inequality (2.9). The lower bound $1 \leq \nu_{k+\ell}(\tilde{\Phi})$ is an immediate consequence of Proposition A.1. For the upper bound, first note that $\nu_{k+\ell}(\tilde{\Phi}) \leq \nu_\ell(\tilde{\Phi}_{(-k)})$ by the Poincaré separation theorem (Theorem A.2). From the expression (2.8) for $\tilde{\Phi}$, we have

$$\begin{aligned}\nu_\ell(\tilde{\Phi}_{(-k)}) &= \nu_\ell(\mathbf{I}_k + \tau^2 \mathbf{\Lambda}_{(-k)} (\mathbf{X}^\top \mathbf{\Omega} \mathbf{X})_{(-k)} \mathbf{\Lambda}_{(-k)}) \\ &= 1 + \tau^2 \nu_\ell(\mathbf{\Lambda}_{(-k)} (\mathbf{X}^\top \mathbf{\Omega} \mathbf{X})_{(-k)} \mathbf{\Lambda}_{(-k)}),\end{aligned}$$

where the second equality follows from Proposition A.1. Applying Lemma A.3 with $\mathbf{A} = (\mathbf{X}^\top \mathbf{\Omega} \mathbf{X})_{(-k)}$ and $\mathbf{B} = \lambda_{(k+1)}^{-2} \mathbf{\Lambda}_{(-k)}^2$, we obtain

$$\nu_\ell(\tilde{\Phi}_{(-k)}) \leq 1 + \tau^2 \lambda_{(k+1)}^2 \nu_\ell((\mathbf{X}^\top \mathbf{\Omega} \mathbf{X})_{(-k)}).$$

Thus we have shown

$$\nu_{k+\ell}(\tilde{\Phi}) \leq 1 + \tau^2 \lambda_{(k+1)}^2 \nu_\ell((\mathbf{X}^\top \mathbf{\Omega} \mathbf{X})_{(-k)}) \leq 1 + \tau^2 \lambda_{(k+1)}^2 \nu_\ell(\mathbf{X}^\top \mathbf{\Omega} \mathbf{X}),$$

where the inequality $\nu_\ell((\mathbf{X}^\top \mathbf{\Omega} \mathbf{X})_{(-k)}) \leq \nu_\ell(\mathbf{X}^\top \mathbf{\Omega} \mathbf{X})$ follows again from the Poincaré separation theorem. \square

Proposition A.1. *Given a $p \times p$ symmetric matrix \mathbf{A} , the eigenvalues of the matrix $\mathbf{I}_p + \mathbf{A}$ are given by $1 + \nu_k(\mathbf{A})$ for $k = 1, \dots, p$.*

Proof. The result follows immediately from the spectral theorem for normal matrices (Horn & Johnson 2012). \square

Theorem A.2 (Poincaré separation theorem). *For a given $p \times p$ symmetric matrix \mathbf{A} , let $\mathbf{A}_{(-k)}$ denote the sub-matrix with the first k rows and columns removed from \mathbf{A} . Then the eigenvalues of \mathbf{A} and $\mathbf{A}_{(-k)}$ satisfies*

$$\nu_{k+\ell}(\mathbf{A}) \leq \nu_\ell(\mathbf{A}_{(-k)}) \leq \nu_\ell(\mathbf{A}) \quad \text{for } \ell = 1, \dots, p - k.$$

Since permuting the rows and columns of \mathbf{A} does not change its eigenvalues, the above inequality in fact holds for any sub-matrix of \mathbf{A} obtained by removing k rows and columns of \mathbf{A} corresponding to a common set of indices j_1, \dots, j_k .

Proof. See Chapter 4.3 of Horn & Johnson (2012). \square

Lemma A.3. *Let \mathbf{A} and \mathbf{B} be $p \times p$ symmetric positive definite matrices and suppose that the largest eigenvalue of \mathbf{B} satisfies $\nu_1(\mathbf{B}) \leq 1$. Then we have*

$$\nu_k(\mathbf{B}^{1/2} \mathbf{A} \mathbf{B}^{1/2}) \leq \nu_k(\mathbf{A}) \quad \text{for } k = 1, \dots, p$$

where $\nu_k(\cdot)$ denotes the k -th largest eigenvalue of a given matrix.

Proof. The result follows immediately from Ostrowski's theorem (Theorem 4.5.9 in Horn & Johnson (2012)). □

Appendix B Theories of CG convergence behavior

In this section, we provide mathematical foundations behind the claims made in Rule of Thumb 2.4. In essence, Rule of Thumb 2.4 is our attempt at describing a phenomenon known as the *super-linear* convergence of CG in a quantitative yet accessible manner. While this is a well-known phenomenon among the researchers in scientific computing, it is rarely explained in canonical textbooks and reference books in numerical linear algebra.² Here we bring together some of the most practically useful results found in the literature and present them in a concise and self-contained manner. Our presentation in Section B.1 and B.2 is roughly based on Section 5.3 of Van der Vorst (2003) with details modified, added, and condensed as needed. More comprehensive treatment of the known results related to CG is found in Meurant (2006). Kuijlaars (2006) sheds additional light on CG convergence behaviors by studying them from the potential theory perspective.

Section B.1 explains the critical first step in understanding the convergence of CG applied to a positive definite system $\Phi \boldsymbol{\beta} = \mathbf{b}$ — relating the CG approximation error to polynomial interpolation error over the set $\{\nu_1, \dots, \nu_p\}$ comprising the eigenvalues of Φ . From this perspective, one can understand Theorem 2.2 as a generic and crude bound, ignoring the distributions of ν_j 's in-between the largest and smallest eigenvalues (Theorem B.3). Theorem 2.3 similarly follows from the polynomial approximation perspective.

²For example, discussions beyond Theorem 2.2 and 2.3 cannot be found in, to name a few, Trefethen & Bau (1997), Demmel (1997), Saad (2003), and Golub & Van Loan (2012).

The effects of the largest eigenvalues on CG convergence, as stated in Rule of Thumb 2.4, is made mathematically precise in Theorem B.4. Analyzing how the smallest eigenvalues delay CG convergence is more involved and requires a discussion of how the eigenvalues are approximated in the Krylov subspace. The amount of initial delay in CG convergence is closely related to how quickly these eigenvalue approximations converge. A precise statement is given in Theorem B.5.

The proofs of all the results stated in this section are provided in Supplement Section S7.

B.1 CG approximation error as polynomial interpolation error

The space of polynomials \mathcal{P}_k as defined below plays a prominent role in the behavior of a worst-case CG approximation error:

$$\mathcal{P}_k = \{Q_k(\nu) : Q_k \text{ is a polynomial of degree } k \text{ with } Q_k(0) = 1\}.$$

Proposition B.1 below establishes the connection between CG and the space \mathcal{P}_k .

Proposition B.1. *The difference between the k -th CG iterate β_k and the exact solution β can be expressed as*

$$\beta_k - \beta = R_k(\Phi)(\beta_0 - \beta) \quad \text{for } R_k = \operatorname{argmin}_{Q_k \in \mathcal{P}_k} \|Q_k(\Phi)(\beta_0 - \beta)\|_{\Phi}. \quad (\text{B.14})$$

In particular, the following inequality holds for any $Q_k \in \mathcal{P}_k$:

$$\|\beta_k - \beta\|_{\Phi} \leq \|Q_k(\Phi)(\beta_0 - \beta)\|_{\Phi}. \quad (\text{B.15})$$

Theorem B.2 below uses Proposition B.1 to establish the relation between the CG approximation error and a polynomial interpolation error. We can interpret the result as saying the following: a worst-case CG approximation error can be quantified via how well the set of points $\{(\nu_j, 0)\}_{j=1, \dots, p}$ can be interpolated by the graph $\nu \rightarrow (\nu, Q_k(\nu))$ of a k -th degree polynomial Q_k with the constraint $Q_k(0) = 1$.

Theorem B.2.

$$\frac{\|\beta_k - \beta\|_{\Phi}}{\|\beta_0 - \beta\|_{\Phi}} \leq \min_{Q_k \in \mathcal{P}_k} \max_{j=1, \dots, p} |Q_k(\nu_j)|, \quad (\text{B.16})$$

where ν_j denotes the j -th largest eigenvalue of Φ . The bound is sharp in a sense that, for each k , there exists an initial vector β_0 for which the equality holds.

B.2 Bounding CG error via its polynomial characterization

We now derive bounds on the CG approximation error through its characterization as a polynomial interpolation error (Theorem B.2). Minimizing the interpolation error over the entire interval between the largest and smallest eigenvalues yields the following bound.

Theorem B.3.

$$\min_{Q_k \in \mathcal{P}_k} \max_{\nu \in [\nu_{min}, \nu_{max}]} |Q_k(\nu)| \leq 2 \left(\frac{\sqrt{\nu_{max}/\nu_{min}} - 1}{\sqrt{\nu_{max}/\nu_{min}} + 1} \right)^k. \quad (\text{B.17})$$

Theorem B.2 and B.3 together yield the well-known CG approximation error bound of Theorem 2.2. As the bound of Theorem B.2 depends only on the maximum over a discrete set of the eigenvalues $\{\nu_p, \dots, \nu_1\}$, rather than the entire interval $[\nu_p, \nu_1]$, the actual CG convergence rate can be faster.

Theorem B.4 below is a basis of the following claim made in Rule of Thumb 2.4: “the r largest eigenvalues are effectively removed within r iterations.”

Theorem B.4. *The following bound holds for all $r, k \geq 0$ with $r < p$:*

$$\frac{\|\beta_{r+k} - \beta\|_{\Phi}}{\|\beta_0 - \beta\|_{\Phi}} = \min_{Q_{r+k} \in \mathcal{P}_{r+k}} \max_{j=1, \dots, p} |Q_{r+k}(\nu_j)| \leq 2 \left(\frac{\sqrt{\nu_{r+1}/\nu_p} - 1}{\sqrt{\nu_{r+1}/\nu_p} + 1} \right)^k, \quad (\text{B.18})$$

where the first equality is given by Theorem B.2.

The smallest eigenvalues affect the CG convergence rate differently from the largest ones due to the constraint $Q_k(0) = 1$ in \mathcal{P}_k . Intuitively, this constraint makes the smallest eigenvalues more significant contributors to the polynomial interpolation error because it competes with the objective of minimizing $|Q_k(\nu)|$ for small ν . This is why we state in Rule of Thumb 2.4 that “the same number of smallest eigenvalues tends to delay the convergence longer.” Nonetheless, the effects of the smallest eigenvalues on the CG approximation error becomes attenuated as the CG iterations proceed. To quantify this phenomenon, we need to introduce the notion of *Ritz values* and describe their roles in the CG convergence behavior.

The Ritz values at the k -th CG iteration refer to the roots $\{\widehat{\nu}_1^{(k)}, \dots, \widehat{\nu}_k^{(k)}\}$ of the optimal CG polynomial R_k as defined in (B.14). Unless the eigenvalues ν_p, \dots, ν_1 are distributed in a highly unusual manner, the largest and smallest Ritz values have a property that they converges quickly to to the largest and smallest eigenvalues of Φ (Trefethen & Bau 1997,

Driscoll et al. 1998, Kuijlaars 2006). More precisely, we have $\widehat{\nu}_i^{(k)} \rightarrow \nu_i$ for $i = 1, \dots, r$ and $\widehat{\nu}_{k-i}^{(k)} \rightarrow \nu_{p-i}$ for $i = 0, \dots, s$ as $k \rightarrow p$. While the convergence rates of the Ritz values can be shown to be exponential, in practice quite a large number of CG iterations may be required to obtain good approximations unless $\max\{r, s\} \ll p$ (Saad 2011).

Theorem B.5 below quantifies how the convergence of the Ritz values are related to the subsequent acceleration of the CG convergence rates.

Theorem B.5. *The CG approximation error of the $(k + \ell)$ -th iterate relative to the k -th iterate satisfies the following bound:*

$$\frac{\|\boldsymbol{\beta}_{k+\ell} - \boldsymbol{\beta}\|_{\Phi}}{\|\boldsymbol{\beta}_k - \boldsymbol{\beta}\|_{\Phi}} \leq C_{k,r,s} 2 \left(\frac{\sqrt{\nu_{r+1}/\nu_{p-s}} - 1}{\sqrt{\nu_{r+1}/\nu_{p-s}} + 1} \right)^{\ell}, \quad (\text{B.19})$$

where $C_{k,r,s} = C_{k,r,s}(\widehat{\nu}_1^{(k)}, \dots, \widehat{\nu}_k^{(k)}) \rightarrow 1$ as $k \rightarrow p$ for any fixed $r, s \geq 0$ with $r + s < p$. More precisely, $C_{k,r,s}$ tends to 1 as the r largest and s smallest Ritz values converge to the largest and smallest eigenvalues of Φ .

References

- Berger, J. O., Bernardo, J. M., Sun, D. et al. (2009), ‘The formal definition of reference priors’, *The Annals of Statistics* **37**(2), 905–938.
- Bhadra, A., Datta, J., Polson, N. G. & Willard, B. T. (2017), ‘Lasso meets horseshoe’, *arXiv:1706.10179*.
- Bhattacharya, A., Chakraborty, A. & Mallick, B. K. (2016), ‘Fast sampling with Gaussian scale mixture priors in high-dimensional regression’, *Biometrika* **103**(4), 985–991.
- Bhattacharya, A., Pati, D., Pillai, N. S. & Dunson, D. B. (2015), ‘Dirichlet–Laplace priors for optimal shrinkage’, *Journal of the American Statistical Association* **110**(512), 1479–1490.
- Carvalho, C. M., Polson, N. G. & Scott, J. G. (2010), ‘The horseshoe estimator for sparse signals’, *Biometrika* **97**(2), 465–480.
- Datta, J., Ghosh, J. K. et al. (2013), ‘Asymptotic properties of Bayes risk for the horseshoe prior’, *Bayesian Analysis* **8**(1), 111–132.

- Demmel, J. W. (1997), *Applied Numerical Linear Algebra*, Vol. 56, Society for Industrial and Applied Mathematics.
- Dongarra, J., Heroux, M. A. & Luszczek, P. (2016), ‘High-performance conjugate-gradient benchmark: A new metric for ranking high-performance computing systems’, *The International Journal of High Performance Computing Applications* **30**(1), 3–10.
- Driscoll, T. A., Toh, K.-C. & Trefethen, L. N. (1998), ‘From potential theory to matrix iterations in six steps’, *SIAM review* **40**(3), 547–578.
- Duff, I. S., Erisman, A. M. & Reid, J. K. (2017), *Direct methods for sparse matrices*, Oxford University Press.
- Geyer, C. (2011), Introduction to Markov chain Monte Carlo, *in* ‘Handbook of Markov Chain Monte Carlo’, CRC Press, pp. 3–48.
- Gibbs, M. & MacKay, D. (1996), Efficient implementation of Gaussian processes. Unpublished manuscript.
- Golub, G. H. & Van Loan, C. F. (2012), *Matrix computations*, Vol. 3, Johns Hopkins University Press.
- Graham, D. J., Reichman, M. E., Wernecke, M., Zhang, R., Southworth, M. R., Levenson, M., Sheu, T.-C., Mott, K., Goulding, M. R., Houstoun, M. et al. (2015), ‘Cardiovascular, bleeding, and mortality risks in elderly Medicare patients treated with dabigatran or warfarin for non-valvular atrial fibrillation’, *Circulation* **131**, 157–164.
- Greenbaum, A. (1979), ‘Comparison of splittings used with the conjugate gradient algorithm’, *Numerische Mathematik* **33**(2), 181–193.
- Hahn, P. R., He, J. & Lopes, H. F. (2018), ‘Efficient sampling for Gaussian linear regression with arbitrary priors’, *Journal of Computational and Graphical Statistics* .
- Hastie, T., Tibshirani, R. & Friedman, J. (2009), *The Elements of Statistical Learning*, Springer Series in Statistics, Springer.
- Hestenes, M. R. & Stiefel, E. (1952), ‘Methods of conjugate gradients for solving linear systems’, *Journal of Research of the National Bureau of Standards* **49**(6).

- Horn, R. A. & Johnson, C. R. (2012), *Matrix Analysis*, Cambridge University Press.
- Hripcsak, G., Duke, J. D., Shah, N. H., Reich, C. G., Huser, V., Schuemie, M. J., Suchard, M. A., Park, R. W., Wong, I. C. K., Rijnbeek, P. R. et al. (2015), ‘Observational Health Data Sciences and Informatics (OHDSI): Opportunities for observational researchers’, *Studies in health technology and informatics* **216**, 574.
- Hripcsak, G., Ryan, P. B., Duke, J. D., Shah, N. H., Park, R. W., Huser, V., Suchard, M. A., Schuemie, M. J., DeFalco, F. J., Perotte, A. et al. (2016), ‘Characterizing treatment pathways at scale using the OHDSI network’, *Proceedings of the National Academy of Sciences* **113**(27), 7329–7336.
- Johndrow, J. E., Orenstein, P. & Bhattacharya, A. (2018), ‘Bayes shrinkage at GWAS scale: Convergence and approximation theory of a scalable MCMC algorithm for the horseshoe prior’, *arXiv:1705.00841* .
- Jolliffe, I. T. (2002), *Principal Component Analysis*, Springer Series in Statistics, Springer.
- Kuijlaars, A. B. J. (2006), ‘Convergence analysis of Krylov subspace iterations with methods from potential theory’, *SIAM review* **48**(1), 3–40.
- Kyung, M., Gill, J., Ghosh, M., Casella, G. et al. (2010), ‘Penalized regression, standard errors, and Bayesian lassos’, *Bayesian Analysis* **5**(2), 369–411.
- Lanczos, C. (1952), ‘Solution of systems of linear equations by minimized iterations’, *Journal of Research of the National Bureau of Standards* **49**(1), 33–53.
- Meurant, G. A. (2006), *The Lanczos and Conjugate Gradient Algorithms: from Theory to Finite Precision Computations*, Society for Industrial and Applied Mathematics.
- Nishimura, A. & Suchard, M. A. (2019), ‘Regularization of Bayesian shrinkage priors and inference via geometrically/uniformly ergodic gibbs sampler’, *arXiv:1911.02160* .
- Pal, S., Khare, K. et al. (2014), ‘Geometric ergodicity for Bayesian shrinkage models’, *Electronic Journal of Statistics* **8**(1), 604–645.
- Park, T. & Casella, G. (2008), ‘The Bayesian Lasso’, *Journal of the American Statistical Association* **103**(482), 681–686.

- Plummer, M., Best, N., Cowles, K. & Vines, K. (2006), ‘Coda: convergence diagnosis and output analysis for MCMC’, *R news* **6**(1), 7–11.
- Polson, N. G., Scott, J. G. & Windle, J. (2013), ‘Bayesian inference for logistic models using Pólya–Gamma latent variables’, *Journal of the American Statistical Association* **108**(504), 1339–1349.
- Polson, N. G., Scott, J. G. & Windle, J. (2014), ‘The Bayesian bridge’, *Journal of the Royal Statistical Society: Series B (Statistical Methodology)* **76**(4), 713–733.
- Rue, H. & Held, L. (2005), *Gaussian Markov random fields: theory and applications*, CRC press.
- Saad, Y. (2003), *Iterative Methods for Sparse Linear Systems*, Vol. 82, Society for Industrial and Applied Mathematics.
- Saad, Y. (2011), *Numerical Methods for Large Eigenvalue Problems: Revised Edition*, Classics in Applied Mathematics, Society for Industrial and Applied Mathematics.
- Schuemie, M. J., Ryan, P. B., Hripcsak, G., Madigan, D. & Suchard, M. A. (2018a), ‘Improving reproducibility by using high-throughput observational studies with empirical calibration’, *Philosophical Transactions of the Royal Society of London A: Mathematical, Physical and Engineering Sciences* **376**(2128), 20170356.
- Schuemie, M. J., Ryan, P. B., Hripcsak, G., Madigan, D. & Suchard, M. A. (2018b), ‘A systematic approach to improving the reliability and scale of evidence from health care data’, *arXiv:1803.10791* .
- Stein, M. L., Chen, J. & Anitescu, M. (2012), ‘Difference filter preconditioning for large covariance matrices’, *SIAM Journal on Matrix Analysis and Applications* **33**(1), 52–72.
- Stroud, J. R., Stein, M. L. & Lysen, S. (2017), ‘Bayesian and maximum likelihood estimation for Gaussian processes on an incomplete lattice’, *Journal of Computational and Graphical Statistics* **26**(1), 108–120.
- Stuart, E. A. (2010), ‘Matching methods for causal inference: A review and a look forward’, *Statistical Science* **25**(1), 1.

- Sun, Y. & Stein, M. L. (2016), ‘Statistically and computationally efficient estimating equations for large spatial datasets’, *Journal of Computational and Graphical Statistics* **25**(1), 187–208.
- Tian, L., Alizadeh, A. A., Gentles, A. J. & Tibshirani, R. (2014), ‘A simple method for estimating interactions between a treatment and a large number of covariates’, *Journal of the American Statistical Association* **109**(508), 1517–1532.
- Tian, Y., Schuemie, M. J. & Suchard, M. A. (2018), ‘Evaluating large-scale propensity score performance through real-world and synthetic data experiments’, *International Journal of Epidemiology* .
- Trefethen, L. N. & Bau, D. (1997), *Numerical Linear Algebra*, Society for Industrial and Applied Mathematics.
- Van der Vorst, H. A. (2003), *Iterative Krylov Methods for Large Linear Systems*, Vol. 13, Cambridge University Press.
- Walker, A. M., Patrick, A. R., Lauer, M. S., Hornbrook, M. C., Marin, M. G., Platt, R., Roger, V. L., Stang, P. & Schneeweiss, S. (2013), ‘A tool for assessing the feasibility of comparative effectiveness research’, *Comparative Effectiveness Research* **3**, 11–20.
- Xu, X., Ghosh, M. et al. (2015), ‘Bayesian variable selection and estimation for group lasso’, *Bayesian Analysis* **10**(4), 909–936.
- Zhang, L., Datta, A. & Banerjee, S. (2018), ‘Practical Bayesian modeling and inference for massive spatial datasets on modest computing environments’, *arXiv:1802.00495* .
- Zhou, Q. & Guan, Y. (2017), ‘Fast model-fitting of Bayesian variable selection regression using the iterative complex factorization algorithm’, *arXiv preprint arXiv:1706.09888* .

Supplement to “Prior-preconditioned conjugate gradient method for accelerated Gibbs sampling in ‘large n & large p ’ sparse Bayesian regression”

S1 General principle behind prior-preconditioning

In the context of the CG sampler, the preconditioned matrix $\mathbf{M}^{-1/2}\tilde{\Phi}\mathbf{M}^{-1/2}$ represents the precision matrix of the transformed parameter $\tilde{\beta} = \mathbf{M}^{1/2}\beta$. In fact, preconditioning the linear system (2.4) with a preconditioner \mathbf{M} is equivalent to applying a parameter transformation $\beta \rightarrow \mathbf{M}^{1/2}\beta$ before employing the CG sampler. That is, we can apply one of the two strategies — precondition the linear system or apply the parameter transformation — to achieve exactly the same effect on the speed of the CG sampler.

When we choose the prior precision as the preconditioner, the transformed parameter $\mathbf{M}^{1/2}\beta$ a priori has the identity precision matrix, before its distribution is modified via the likelihood. This perspective, combined with the fact that the eigenvalues of $\tilde{\Phi}$ represents the posterior precisions of $\mathbf{M}^{1/2}\beta$ along its principal components, suggests the following principle:

Principle Behind Prior-preconditioning S1.1. *Under a strongly informative prior, the posterior looks like the prior except in a small number of directions along which the data provide significant information. This translates into the eigenvalues of the prior-preconditioned matrix $\tilde{\Phi}$ clustering around 1 except for a relatively small number of large eigenvalues.*

The eigenvalue structure of the prior-preconditioned matrix as predicted above is indeed observed across all of our numerical examples — see Figure 3.3, S5, and S6.

S2 Practical details on deploying CG sampler for sparse regression

Throughout this section, we write \mathbf{vw} and \mathbf{v}/\mathbf{w} to denote an element-wise multiplication and division of two vectors \mathbf{v} and \mathbf{w} .

S2.1 Choice of initial vector for CG iterations

Generally speaking, the CG iterations decrease the distance between the iterates β_k 's and the exact solution β relative to the initial error $\|\beta_0 - \beta\|_{\Phi}$. However, a choice of the initial vector is not as significant as that of the preconditioner which determines the eventual exponential convergence rate of CG. In other words, once the initial vector is chosen within a reasonable range, we should not expect a dramatic gain from further fine-tuning. When sampling β from a sparse regression posterior, we indeed find it difficult to improve much over a simple initialization $\beta_0 = \mathbf{0}$, which is a reasonable choice as most coefficients are shrunk to zero. We achieve only small ($\lesssim 10\%$), though consistent, improvements by one of the alternative approaches we experimented with. We describe these approaches below.

As an alternative to $\beta_0 = \mathbf{0}$, we consider three approaches for constructing the initial vector. At the m -th Gibbs update, the CG sampler needs to draw $\beta^{(m)}$ from the distribution $\beta | \omega^{(m-1)}, \lambda^{(m-1)}, \tau^{(m-1)}, \mathbf{y}, \mathbf{X}$. We have no control over the variability in $\beta^{(m)}$, so we focus on getting β_0 as close as possible to the mean of $\beta^{(m)}$. The two seemingly obvious choices of β_0 are 1) the previous MCMC sample $\beta^{(m-1)}$ and 2) the MCMC estimate $m^{-1} \sum_{i=0}^{m-1} \beta^{(i)}$ of the expectation $\mathbb{E}[\beta | \mathbf{y}, \mathbf{X}]$. These options, however, ignores the fact that the distribution of $\beta^{(m)}$ depends strongly on $\tau^{(m-1)}\lambda^{(m-1)}$, which generally is very different from $\tau^{(m-i)}\lambda^{(m-i)}$ for $i \geq 2$.

We found the following approach, implemented in our CG-accelerated Gibbs sampler of Section 4, to yield a better estimate of the mean and hence a better initialization for $\beta^{(m)}$. We first estimate $\mathbb{E}[\tau^{-1}\lambda^{-1}\beta | \mathbf{y}, \mathbf{X}]$ by the estimator $\tilde{\beta}_0 = m^{-1} \sum_{i=0}^{m-1} \beta^{(i)} / \tau^{(i-1)}\lambda^{(i-1)}$, where we define $\tau^{(-1)}\lambda_j^{(-1)} = 1$. Then we rescale it with the current conditioned values of τ and λ , setting $\beta_0 = \tau^{(m-1)}\lambda^{(m-1)}\tilde{\beta}_0$ to obtain the initial vector. We compared this approach to

the other two through a simulation study and found our choice to consistently yield smaller Φ -norm errors and faster convergence.

S2.2 Termination criteria for CG iterations

An iterative method must be supplied with a termination criteria to decide when the current iterate β_k is close enough to the exact solution. While different convergence metrics can be computed as bi-products of the CG iterations (Meurant 2006), most existing linear algebra libraries uses the ℓ^2 norm of the residual $\mathbf{r}_k = \Phi\beta_k - \mathbf{b}$. It is possible to relate the residual norm to $\|\beta_k - \beta\|_2$ as

$$\|\beta_k - \beta\|_2 = \|\Phi^{-1}\mathbf{r}_k\|_2 \leq \|\Phi^{-1}\|_2 \|\mathbf{r}_k\|_2.$$

For the purpose of sampling a Gaussian vector β , however, it is not at all clear when $\|\mathbf{r}_k\|_2$ or $\|\beta_k - \beta\|_2$ can be considered small enough. To address this problem, we develop an alternative metric tailored toward the CG sampler for sparse regression.

We propose to assess the CG convergence in terms of the ℓ^2 norm of the prior-preconditioned residual $\tilde{\mathbf{r}}_k = \tilde{\Phi}\tilde{\beta}_k - \tilde{\mathbf{b}} = \tau\lambda\mathbf{r}_k$. More specifically, we use the termination criteria

$$p^{-1/2}\|\tilde{\mathbf{r}}_k\|_2 = \left\{ p^{-1} \sum_{j=1}^p (\tilde{\mathbf{r}}_k)_j^2 \right\}^{1/2} \leq 10^{-6}, \quad (\text{S1})$$

in terms of the root-mean-squared residual $p^{-1/2}\|\tilde{\mathbf{r}}_k\|_2$. The criteria is justified by the norm $\|\tilde{\mathbf{r}}_k\|_2$ being an approximate upper bound to the following quantity:

$$\|\xi^{-1}(\beta_k - \beta)\|_2 \quad \text{with} \quad \xi_j^2 = \mathbb{E}[\beta_j^2 | \omega, \lambda, \tau, \mathbf{y}, \mathbf{X}]. \quad (\text{S2})$$

The standardization by second moment ensures that, when the computed error is small, all the coordinates of β_k are close to those of β either in terms of their means or variances of the target Gaussian distribution.

To relate the norm of the prior-preconditioned residual $\tilde{\mathbf{r}}_k = \tilde{\Phi}\tilde{\beta}_k - \tilde{\mathbf{b}}$ to the error metric (S2), observe that $\beta_k - \beta = \mathbf{M}^{-1/2}\tilde{\Phi}^{-1}\tilde{\mathbf{r}}_k$ with $\mathbf{M} = \tau^{-2}\Lambda^{-2}$ and hence

$$\|\xi^{-1}(\beta_k - \beta)\|_2 = \|\xi^{-1}(\tau\lambda)(\tilde{\Phi}^{-1}\tilde{\mathbf{r}}_k)\|_2 \leq \left(\max_j \xi_j^{-1}\tau\lambda_j \right) \|\tilde{\Phi}^{-1}\tilde{\mathbf{r}}_k\|_2. \quad (\text{S3})$$

The inequality in the above equation only represents the worst-case scenario; in more typical settings, one expects the norm of $\xi^{-1}(\tau\lambda)\mathbf{v}$ to be related to that of \mathbf{v} through some average of

$\xi_j^{-1}\tau\lambda_j$'s. In any case, we proceed to analyze a typical behavior of $\xi_j^{-1}\tau\lambda_j$ as the parameters $\boldsymbol{\omega}, \boldsymbol{\lambda}, \tau$ are drawn from a sparse regression posterior. As before, we interpret $\tau^2\lambda_j^2$ as the prior variance of β_j (conditional on $\boldsymbol{\omega}, \boldsymbol{\lambda}, \tau$) before observing \mathbf{y}, \mathbf{X} . Note that

$$(\xi_j^{-1}\tau\lambda_j)^2 = \frac{\tau^2\lambda_j^2}{\mu_j^2 + \sigma_j^2},$$

where μ_j and σ_j are the conditional mean and variance of $\beta_j \mid \boldsymbol{\omega}, \boldsymbol{\lambda}, \tau, \mathbf{y}, \mathbf{X}$. So the quantity $\xi_j^{-1}\tau\lambda_j$ is not too far from 1 if either $|\mu_j|$ or σ_j is in the same order of magnitude as $\tau\lambda_j$. If β_j 's posterior is dominated by the prior shrinkage, we expect the posterior (conditional) variance to be not much smaller than the prior one and hence $\sigma_j \approx \tau\lambda_j$. Otherwise, if $\sigma_j \ll \tau\lambda_j$ and the likelihood is a dominant contributor to the posterior, then the posterior of $\tau\lambda_j$ should concentrate around of $|\mu_j|$ to maximize the marginal likelihood of $\beta_j \approx \mu_j$. Either way, we can expect $\xi_j^{-1}\tau\lambda_j$ to be in the same order of magnitude as 1.

From the relation (S3) and our analysis above, we deduce that

$$\|\boldsymbol{\xi}^{-1}(\boldsymbol{\beta}_k - \boldsymbol{\beta})\|_2 \lesssim \|\tilde{\boldsymbol{\Phi}}^{-1}\tilde{\mathbf{r}}_k\|_2 \leq \|\tilde{\mathbf{r}}_k\|_2,$$

where the latter inequality follows from the fact that the largest eigenvalue of the prior-preconditioned matrix $\tilde{\boldsymbol{\Phi}}^{-1}$ is bounded above by 1 by Theorem 2.5.

S2.3 Modified preconditioner to handle coefficients with uninformative priors

When fitting a sparse regression model, standard practice is to include an intercept β_0 without any shrinkage, often with the improper flat prior $\pi(\beta_0) \propto 1$ (Park & Casella 2008). Additionally, there may be predictors of particular interests, inference for whose regression coefficients is more appropriately carried out with uninformative or weakly-informative priors without shrinkage; see Zucknick et al. (2015) as well as the application in Section 4 for examples of such predictors. The CG sampler can accommodate such predictors with an appropriate modification.

For notational convenience, suppose that the regression coefficients are indexed so that the first $(q+1)$ -th coefficients $\beta_0, \beta_1, \dots, \beta_q$ are to be estimated without shrinkage. We further

assume that the unshrunk coefficients are given independent Gaussian priors $\beta_j \sim \mathcal{N}(0, \sigma_j^2)$ for $0 < \sigma_j \leq \infty$ where $\sigma_j = \infty$ denotes an improper prior $\pi(\beta_j) \propto 1$. The precision matrix of $\boldsymbol{\beta} | \boldsymbol{\omega}, \boldsymbol{\lambda}, \tau, \mathbf{y}, \mathbf{X}$ then is given by

$$\boldsymbol{\Phi} = \mathbf{X}^\top \boldsymbol{\Omega} \mathbf{X} + \begin{bmatrix} \text{diag}(\boldsymbol{\sigma})^{-2} & \mathbf{0} \\ \mathbf{0} & \tau^{-2} \boldsymbol{\Lambda}^{-2} \end{bmatrix}$$

for $\boldsymbol{\sigma} = (\sigma_0, \dots, \sigma_q)$ where we employ the convention $1/\sigma_j = 0$ if $\sigma_j = \infty$. The unshrunk coefficients β_0, \dots, β_q are distinguished from the shrunk ones by the fact that their prior scales σ_j (before conditioning on \mathbf{y} and \mathbf{X}) typically have little to do with their posterior scales (after conditioning on \mathbf{y} and \mathbf{X}). For this reason, a naively modified preconditioner $\mathbf{M} = \text{diag}(\boldsymbol{\sigma}^{-2}, \tau^{-2} \boldsymbol{\Lambda}^{-2})$ may not be appropriate, especially for coefficients with $\sigma_j \gg 1$ corresponding to uninformative priors.

We propose a modified preconditioner of the form $\mathbf{M} = \text{diag}(\boldsymbol{\gamma}^{-2}, \tau^{-2} \boldsymbol{\Lambda}^{-2})$ for appropriately chosen $\boldsymbol{\gamma} = (\gamma_0, \gamma_1, \dots, \gamma_q)$. For the corresponding preconditioned matrix $\tilde{\boldsymbol{\Phi}} = \mathbf{M}^{-1/2} \boldsymbol{\Phi} \mathbf{M}^{-1/2}$, let $\tilde{\boldsymbol{\Phi}}_{(-q-1)}$ denote the sub-matrix with the first $q+1$ rows and columns removed. As shown in Section 2.5, the sub-matrix $\tilde{\boldsymbol{\Phi}}_{(-q-1)}$ has an eigenvalue distribution particularly well-suited to induce rapid CG convergence. By the Poincaré separation theorem (Theorem A.2), all but $q+1$ eigenvalues of the original matrix $\tilde{\boldsymbol{\Phi}}$ lie within the largest and smallest eigenvalues of the sub-matrix $\tilde{\boldsymbol{\Phi}}_{(-q-1)}$. In choosing γ_j 's, therefore, we are concerned with the behavior of the $q+1$ additional eigenvalues introduced by the unshrunk coefficients. Additionally, we should err on the side of introducing larger eigenvalues than smaller ones as small eigenvalues impact CG convergence rates more significantly (Rule of Thumb 2.4).

With the above objectives in mind, we propose a choice

$$\gamma_j = c \hat{\psi}_j \quad \text{for } \hat{\psi}_j^2 \approx \text{var}(\beta_j | \boldsymbol{\omega}, \boldsymbol{\lambda}, \tau, \mathbf{y}, \mathbf{X}) \quad \text{and } c \geq 1. \quad (\text{S4})$$

To explain the reasoning behind the above choice, let $\boldsymbol{\beta}_q = (\beta_0, \dots, \beta_q)$ and $\boldsymbol{\beta}_{(-q)} = (\beta_{q+1}, \dots, \beta_p)$. The smallest eigenvalues of $\tilde{\boldsymbol{\Phi}}$ correspond to the largest variances (conditional on $\boldsymbol{\omega}, \boldsymbol{\lambda}, \tau, \mathbf{y}, \mathbf{X}$) of the Gaussian vector $\mathbf{M}^{1/2} \boldsymbol{\beta} = (\boldsymbol{\gamma}^{-1} \boldsymbol{\beta}_q, \tau^{-1} \boldsymbol{\Lambda}^{-1} \boldsymbol{\beta}_{(-q)})$ along its principal components. The variances of $\tau^{-1} \boldsymbol{\Lambda}^{-1} \boldsymbol{\beta}_{(-q)}$ conditional on $\boldsymbol{\gamma}^{-1} \boldsymbol{\beta}_q$ are bounded above by 1 along any directions because the eigenvalues of the conditional precision matrix $\tilde{\boldsymbol{\Phi}}_{(-q)}$ are bounded below by 1. Therefore, we do not expect $(\boldsymbol{\gamma}^{-1} \boldsymbol{\beta}_q, \tau^{-1} \boldsymbol{\Lambda}^{-1} \boldsymbol{\beta}_{(-q)})$ to have variances

much larger than 1 unless the marginal variances of $\boldsymbol{\gamma}^{-1}\boldsymbol{\beta}_q$ are large. The proposed choice of γ_j 's ensure that the marginal variances of $\gamma_j^{-1}\beta_j$'s are less than c^{-1} and thus prevent an introduction of small eigenvalues to $\tilde{\boldsymbol{\Phi}}$. The multiplicative factor $c \geq 1$ provides a further safeguard as we are more concerned about small eigenvalues than large ones.

As the parameters $\boldsymbol{\omega}, \tau, \boldsymbol{\lambda}$ are constantly updated during Gibbs sampling, technically we cannot estimate $\text{var}(\beta_j | \boldsymbol{\omega}, \boldsymbol{\lambda}, \tau, \mathbf{y}, \mathbf{X})$ from earlier MCMC samples. In practice, we instead use

$$\gamma_j = c \hat{\eta}_j \quad \text{for} \quad \hat{\eta}_j^2 \approx \text{var}(\beta_j | \mathbf{y}, \mathbf{X}). \quad (\text{S5})$$

Using (S5) in place of (S4) is justified in two ways. First, by the variance decomposition formula we have

$$\mathbb{E}_{\boldsymbol{\omega}, \tau, \boldsymbol{\lambda} | \mathbf{y}, \mathbf{X}} [\text{var}(\beta_j | \boldsymbol{\omega}, \boldsymbol{\lambda}, \tau, \mathbf{y}, \mathbf{X})] \leq \text{var}(\beta_j | \mathbf{y}, \mathbf{X}).$$

In other words, on average $\hat{\eta}_j$ is an overestimate of $\hat{\psi}_j$ which, as we have discussed, is more preferable to an underestimate. Secondly, the unshrunk coefficients β_0, \dots, β_q have only limited dependency on the shrinkage parameters τ and $\boldsymbol{\lambda}$ through $\beta_{q+1}, \dots, \beta_p$. Also, in our experience we have never noticed any obvious correlations between the posterior samples of $\boldsymbol{\omega}$ and $\boldsymbol{\beta}$. For these reasons, we suspect that $\text{var}(\beta_j | \mathbf{y}, \mathbf{X})$ is generally not too far from $\text{var}(\beta_j | \boldsymbol{\omega}, \boldsymbol{\lambda}, \tau, \mathbf{y}, \mathbf{X})$.

Once chosen within reasonable ranges, the precise values of γ_j 's have limited effect on the CG convergence rate. This is because all but $(q+1)$ eigenvalues are well-behaved regardless of the choice of $\gamma_0, \dots, \gamma_q$ and CG has an ability to eventually “remove” the extreme eigenvalues (Rule of Thumb 2.4). In our simulations (not presented in the manuscript), we found the delay in the CG convergence to be no more than 20 ~ 30% even when the values of γ_j 's were off by two orders of magnitude from empirically-determined optimal values. The convergence rate achieved by the proposed choice of $\boldsymbol{\gamma}$ was essentially indistinguishable from that achieved by an optimal choice.

S3 Effects of error metrics and right-hand vectors on CG sampler convergence behaviors of Section 3.3

The CG convergence behavior as illustrated in Figure 3.1 remains qualitatively consistent across different random draws of the right-hand vector \mathbf{b} and across various metrics of the approximation error. Figure S1 shows the average of the coordinate-wise relative error as a function of the CG iterations as in Figure 3.1, but with an individual line for each of the random draws of \mathbf{b} . The convergence behaviors under the prior and Jacobi preconditioners are plotted in the two separate sub-figures to avoid cluttering the plot with too many lines. Figure S2 shows the CG convergence behaviors under the two additional error metrics: the ℓ^2 -norm and Φ -norm distance between β_k and β_{direct} .

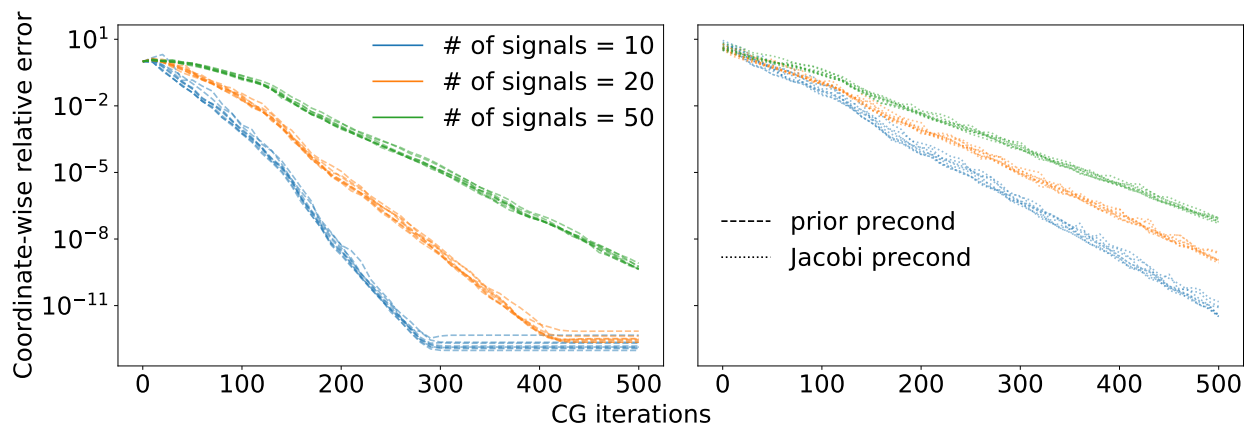


Figure S1: Plots of the CG approximation errors (with the same error metric as used in Figure 3.1) as a function of the number of CG iterations. Shown on the left is under the prior preconditioner and on the right is under the Jacobi preconditioner. The three different colors corresponds to the three different posterior conditional distributions of β with the varying numbers of true signals. Within the same color, the different lines correspond to the different random draws of the right-hand vector \mathbf{b} generated as in (2.3).

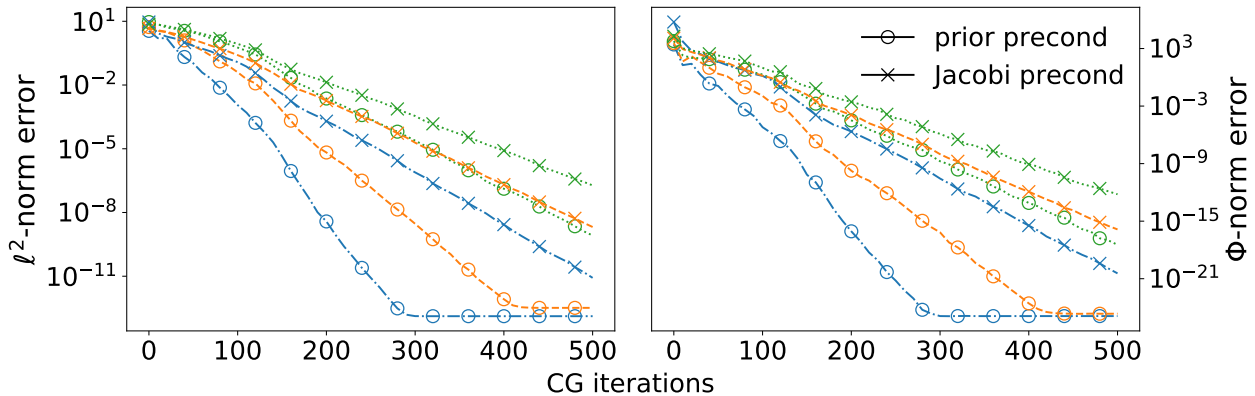


Figure S2: Plots of the ℓ^2 -norm (on the left) and the Φ -norm (on the right) between β_k and β_{direct} as a function of the number of CG iterations. Other than the use of the two alternative error metrics for the y -axes, each of the plotted lines directly corresponds to the one with the same color and marker in Figure 3.1.

S4 Optimizing linear algebra computations for Gibbs samplers

S4.1 Dense vs. sparse numerical linear algebra

When a design matrix \mathbf{X} is sparse as in the application of Section 4, one may wonder if the precision matrix Φ can be factorized efficiently using sparse numerical linear algebra techniques. This is not the case in typical sparse regression applications, however, for the following reasons. First, the matrix $\mathbf{X}^\top \Omega \mathbf{X}$ and hence Φ is typically much denser than \mathbf{X} itself, especially when $n > p$. In particular, the (j, j') -th element of $\mathbf{X}^\top \Omega \mathbf{X}$ is non-zero if the j -th and j' -th predictors co-occur in any of the n samples. Secondly, when employing sparse methods, time spent on irregular data access completely dominate over that on arithmetic operations (Duff et al. 2017). In the absence of sufficient sparsity, therefore, it can be more computationally efficient to ignore the sparse structure and employ dense methods.

In the application of Section 4, we find the precision matrix Φ to be 85.4% dense. The Cholesky factor of a sparse matrix is typically denser than the matrix itself (see Theorem 2.8 in Rue & Held, 2005); indeed, we find the Cholesky factor \mathbf{L} to be over 99% dense. Sparse

methods have no advantage whatsoever for such a dense matrix.

Conceivably, we can avoid dealing with the near-dense Φ matrix in (2.4) as follows. Noting that $\Phi = \tilde{\mathbf{X}}^\top \tilde{\mathbf{X}}$ for $\tilde{\mathbf{X}}^\top = [\mathbf{X}^\top, \tau^{-1} \mathbf{\Lambda}^{-1}]$, we see that a (Q -less) QR decomposition of the sparse matrix $\tilde{\mathbf{X}}$ would provide the Cholesky factor of Φ . For the application of Section 4, we experimented with this idea using the popular SparseSuites package (Davis 2011). Sparse QR decomposition first attempts to find a permutation of the matrix columns to reduce the subsequent computation as much as possible. The package implements approximate minimum degree (AMD), column AMD (COLAMD), as well as graph-partitioning-based nested dissection (METIS) algorithm. None of these algorithms find column orderings that differ significantly from the original arbitrary ordering with only handful of columns permuted. The subsequent factorization of the matrix requires about 25 minutes regardless of the column permutation algorithm chosen. On the other hand, explicitly computing Φ and finding its Cholesky factor via dense linear algebra requires about 3 minutes only (Section S4.2).

S4.2 Choice of linear algebra library

For linear algebra operations involving large matrices, hardware-specific compilation and optimization are essential for achieving good computational efficiency. Major linear algebra libraries all achieve reasonable computational efficiency, but some variation in performance may occur depending on types of operations and computing environments. We therefore compare a few options for implementing the direct and CG-accelerated Gibbs sampler in Section 4. Efficiency of sparse matrix operations also depends critically on the underlying representations of sparse matrices (Saad 2011). For each linear algebra library, we try all the major sparse matrix formats and report only the result with best performance. All the benchmarks here are run using the design matrix of Section 4.

The computational bottleneck of the direct Gibbs sampler is computing $\mathbf{X}^\top \mathbf{\Omega} \mathbf{X}$ and the subsequent Cholesky factorization of Φ . Since $\mathbf{\Omega}$ is a diagonal matrix, computing $\mathbf{X}^\top \mathbf{\Omega} \mathbf{X}$ can be carried out as multiplying a sparse matrix $\mathbf{X}^\top \mathbf{\Omega}^{1/2}$ with its transpose. The high-performance computing community refers to the operation of multiplying two sparse matrices by the acronym SpGEMM (generalized sparse matrix-matrix multiplication). SpGEMM is a surprisingly complicated operation to optimize in modern computing architectures. No

specification is provided for such an operation by sparse BLAS (Duff et al. 2002), and its hardware-specific implementation is an active area of research (Matam et al. 2012, Azad et al. 2016).

The Scipy library provides an SpGEMM implementation via the algorithm of Bank & Douglas (1993). The Scipy SpGEMM operation requires 144 seconds. We find an alternative implementation in the Intel MKL library with the option of returning a dense (instead of sparse) matrix, which is faster here as the multiplied matrix is almost completely dense. The MKL SpGEMM requires 64.6 seconds, being a clear winner and our choice for the simulation results of Section 4.

For the (dense linear algebra) Cholesky factorization of Φ , the Scipy library by default calls the MKL library. The computation requires 78.0 seconds. The OpenBLAS implementation performs comparably, requiring 79.0 seconds.

The computation time of the CG-accelerated Gibbs is dominated by the (sparse) matrix-vector multiplications $\mathbf{v} \rightarrow \mathbf{X}\mathbf{v}$ and $\mathbf{w} \rightarrow \mathbf{X}^T\mathbf{w}$ required for CG iterations. For these operations, the Scipy library uses its own C-extension code. On average, the operation $\mathbf{v} \rightarrow \mathbf{X}\mathbf{v}$ requires 6.70×10^{-2} seconds and the operation $\mathbf{w} \rightarrow \mathbf{X}^T\mathbf{w}$ 6.07×10^{-2} seconds. With the MKL library implementations, these matrix-vector multiplications on average require 4.69×10^{-2} and 5.49×10^{-2} seconds respectively.

S4.3 Opportunities for parallelization within memory constraints

The above comparisons of computational efficiency are based on a single-threaded CPU computing environment. Computational gain from parallelization is highly architecture dependent for large-scale problems and is difficult to draw any general conclusions (Dongarra et al. 2016, Duff et al. 2017). Nonetheless, here we provide a qualitative discussion of to what extent each algorithm can benefit from parallelization. We complement the discussion with illustrative quantitative results, obtained by using all the four Intel CPU's of the 2015 iMac.

Before any discussion of computational gains from parallelization, we emphasize the following point regarding the two alternative Gibbs samplers for sparse Bayesian regression: as the problem size grows, memory constraints make the CG-accelerated sampler *the only option* in a typical computing environment. We can run the CG-accelerated sampler as long

as we have enough memory to store the (sparse) design matrix \mathbf{X} . On the other hand, as we have discussed, the direct Gibbs sampler generally cannot avoid having to store the near-dense precision matrix Φ . In case of the sparse design matrix \mathbf{X} of size $72,489 \times 22,175$ in Section 4, for example, storing \mathbf{X} in the compressed sparse row format only requires 0.719GB of memory while storing the dense Φ requires 3.67GB of memory. In fact, further memory burden is incurred by temporary allocation of extra memory necessary for the Cholesky factorization of Φ . Profiling the memory usage by the MKL library reveal that temporary memory allocation of 3.75GB, requiring at least 8.14 ($= 0.719 + 3.67 + 3.75$) GB of memory for running the direct Gibbs sampler.

Dense linear algebra operations benefit most from parallelization when using a typical modern hardware, which performs best at accessing data stored contiguously in memory (Dongarra et al. 2016). In fact, computation time for the Cholesky factorization goes down from 78.0 to 22.7 seconds when using the four CPU’s with the MKL library. It is also worth noting that the speed-up is significantly smaller when using the OpenBLAS library; the time goes down from 79.0 only to 33.1 seconds, illustrating the importance of hardware-specific optimizations in parallel computing.

Parallelizing sparse linear algebra operations are more complex due to their bottleneck being irregular data access (Duff et al. 2017). Speed-ups thus tend to be smaller, though there are growing efforts in building hardwares optimized for sparse operations (Dongarra et al. 2016). The MKL SpGEMM delivers a modest speed-up when using the four CPU’s, cutting the time from 64.6 to 46.8 seconds. The sparse matrix-vector multiplications $\mathbf{v} \rightarrow \mathbf{X}\mathbf{v}$ and $\mathbf{w} \rightarrow \mathbf{X}^T\mathbf{w}$ benefit slightly more from parallelization. The MKL library implementations reduces the time from 4.69×10^{-2} to 3.13×10^{-2} seconds and from 5.49×10^{-2} to 3.14×10^{-2} seconds respectively.

S5 In-depth look at mechanism of CG-acceleration in Section 4

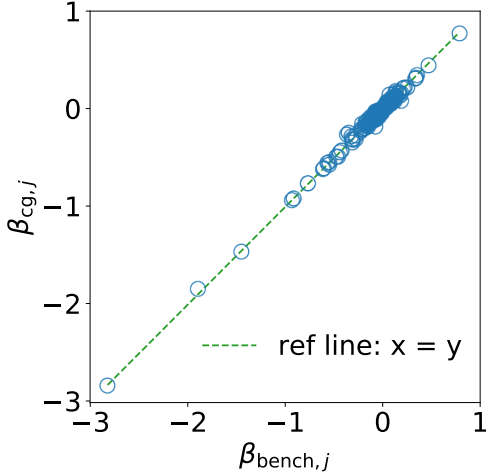
S5.1 Accuracy of CG sampler

Since CG technically does not yield the exact solution when terminated at $k < p$ iterations, we assess the accuracy of the samples generated by the CG-accelerated Gibbs by comparing them against the “ground truth” samples generated by the direct Gibbs. As we show, perturbation of the target distribution due to the CG approximation error is, if any, so small that it is essentially negligible.

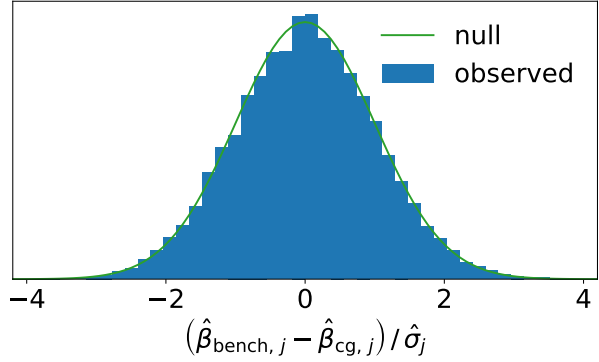
We compare the two sets of samples in terms of the primary parameter of interest β . The mixing of β is generally fast for any fixed τ , but the dependency between β and τ somewhat reduces the overall mixing rate. To ensure that the effective sample sizes for β are large enough to adequately characterize the stationary distribution, therefore, we employ an empirical Bayes approach. We first find a value $\hat{\tau}$ which approximately maximizes the marginal likelihood through Monte Carlo expectation-maximization algorithm (Park & Casella 2008). We then run the two samplers conditional on $\tau = \hat{\tau}$.

We test for differences between the two sets of the MCMC samples as follows. We first set $\hat{\beta}_{\text{bench}}$ and $\hat{\beta}_{\text{cg}}$ to be the posterior means estimated by averaging the samples from the direct Gibbs (used as a benchmark) and CG-accelerated Gibbs. Figure S3(a) graphically compares these two estimators as an informal sanity check. We then estimate the effective sample sizes of β_j from the respective samplers using the R CODA package (Plummer et al. 2006). These estimated effective sample sizes can be used to estimate the Monte Carlo standard deviations $\hat{\sigma}_j$ of the differences $\hat{\beta}_{\text{bench},j} - \hat{\beta}_{\text{cg},j}$. When the two sets of samples have the same stationary distribution, the standardized differences $(\hat{\beta}_{\text{bench},j} - \hat{\beta}_{\text{cg},j})/\hat{\sigma}_j$ are approximately distributed as the standard Gaussians by the Markov chain central limit theorem (Geyer 2011).

Figure S3(b) confirms that the distribution of the standardized differences closely follows the “null” distribution. Figure S3(a) and S3(b) are based on the posterior samples for the propensity score model, but we obtained essentially the same result under the treatment effect



(a) Comparison of the regression coefficient estimates (posterior means) between those based on the direct and CG-accelerated Gibbs samplers.



(b) Normalized histogram for the standardized differences $(\hat{\beta}_{\text{bench},j} - \hat{\beta}_{\text{cg},j})/\hat{\sigma}_j$, where $\hat{\sigma}_i^2$ is an estimate of the Monte Carlo variance of $\hat{\beta}_{\text{bench},j} - \hat{\beta}_{\text{cg},j}$. Gaussianness of the histogram indicates no statistically significant difference between the two MCMC outputs.

Figure S3: Diagnostic plots to check for statistically significant differences between the two MCMC outputs.

model. We additionally performed the same diagnostic on the estimators of the posterior second moment of β and obtained similar results.

S5.2 Number of CG iterations at each Gibbs step

To study computational cost of the CG sampler at each Gibbs iteration, we first focus on a post-burn-in update of β for the propensity score model. As in Section 3, we compare the CG iterates β_k against the exact solution β_{direct} of the linear system (2.4) found via the Cholesky-based direct method. Figure S4 plots the distances between β_k and β_{direct} as a function of k , the number of CG iterations or equivalently of matrix vector multiplications $v \rightarrow \Phi v$.

The solid blue line tracks the root mean squared residual $p^{-1/2} \|\tilde{r}_k\|_2$ as introduced in Section S2.2. The dotted vertical line indicates when the magnitude of the prior-preconditioned residual \tilde{r}_k falls below the termination criteria of (S1). The termination occurs at $k = 133$ and the CG sampler consequently spends less than 10% of the computational time relative

to the direct sampler. Note also how the solid blue line upper-bound the dashed one which tracks the following error metric computed as a proxy for (S2):

$$\left\{ p^{-1} \sum_j \hat{\xi}_j^{-2} (\beta_k - \beta_{\text{direct}})_j^2 \right\}^{1/2} \quad \text{with} \quad \hat{\xi}_j^2 \approx \mathbb{E}[\beta_j^2 | \mathbf{y}, \mathbf{X}]. \quad (\text{S6})$$

This empirical result provides a further support to our theoretical analysis in Section S2.2 and hence to the use of $p^{-1/2} \|\tilde{\mathbf{r}}_k\|_2$ in the termination criteria. As confirmed in Section S5.1, the CG error at termination is so small that it does not affect the stationary distribution of the Gibbs sampler in any statistically significant way.

Figure S4 also makes it clear that the advantage of the prior preconditioner, as demonstrated in the simulated data examples of Section 3, continues to hold in this real data example. The observed convergence behaviors under the two preconditioners are again well explained by the eigenvalue distributions of the respective preconditioned matrices (Figure S5); prior preconditioning leads to a tighter cluster of the eigenvalues and avoids introducing small eigenvalues.

We have so far studied the mechanism of CG-acceleration by using the propensity score model example. For the treatment effect model, the Jacobi preconditioner turns out to be comparable the prior preconditioner because the precision matrix $\Phi = \mathbf{X}^\top \Omega \mathbf{X} + \tau^{-2} \Lambda^{-2}$ is so strongly dominated by the diagonal terms. This phenomenon is explained by the following two facts. First, the posterior is extremely sparse (Section 4.4) and correspondingly the majority of $\tau\lambda$'s are also extremely small. This makes the diagonal prior shrinkage term $\tau^{-2} \Lambda^{-2}$ far more significant than the non-diagonal likelihood term $\mathbf{X}^\top \Omega \mathbf{X}$. Secondly, the entries of $\Omega = \text{diag}(\omega)$, which can be interpreted as the weight on or informativeness of the observation \mathbf{y} (Equation 1.1), are typically quite small due to the low incidence rate (Section 4.1). This further reduces the contribution of the non-diagonal term $\mathbf{X}^\top \Omega \mathbf{X}$ to the precision Φ .

S6 Issue with approximating $\tilde{\Phi}$ by thresholding $\tau\lambda_j$'s

In Section 2.4, we observed that the (i, j) -th entry of $\tau^2 \Lambda \mathbf{X}^\top \Omega \mathbf{X} \Lambda$ is small whenever $\tau\lambda_i \approx 0$ or $\tau\lambda_j \approx 0$. Given this observation, one may wonder if we can obtain a convenient low-rank

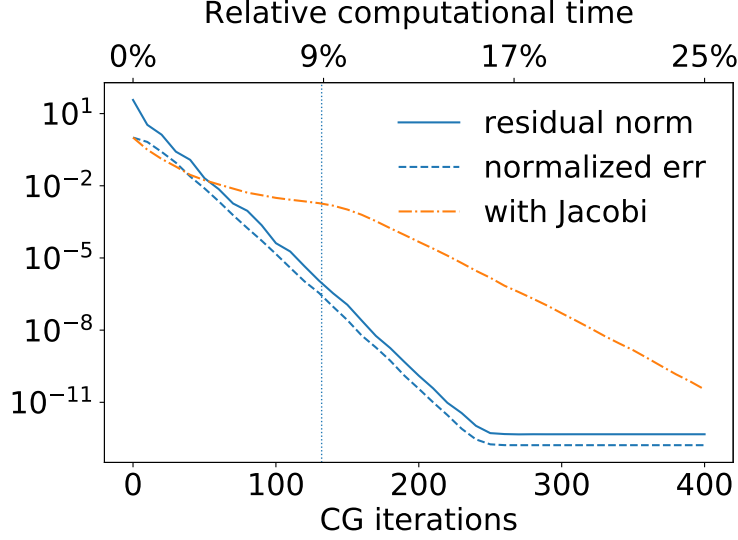


Figure S4: Plot of the CG errors during a conditional update of β within the propensity score model posterior computation. The errors are plotted as a function of the number of CG iterations (bottom axis) and of the computational time relative to the direct linear algebra (top axis). The solid line shows the root mean squared residual $p^{-1/2}\|\tilde{\mathbf{r}}_k\|_2$ used in the stopping criteria (S1). The dotted vertical line indicates when $p^{-1/2}\|\tilde{\mathbf{r}}_k\|_2$ reaches the threshold 10^{-6} . The 2nd-moment normalized errors (S6) are shown as the blue dashed line for the prior preconditioner and as the orange dash-dot line for the Jacobi preconditioner.

approximation of the prior-preconditioned matrix $\tilde{\Phi} = \tau^2 \Lambda \mathbf{X}^\top \Omega \mathbf{X} \Lambda + \mathbf{I}_p$ by zeroing out $\tau \lambda_j$'s at some threshold. This is *not* the case in general as we will show now. Intuitively, the problem is as follows: while the ordered local scale parameter $\lambda_{(k)}$ decays reasonably quickly as k increases, there is no clear “gap” where $\lambda_{(k+1)} \ll \lambda_{(k)}$. For example, the histogram of a posterior draw of $\tau \lambda_j$'s in Figure 3.4 shows clearly that there is no such gap.

We can assess the quality and utility of the thresholding approximation by using it as a preconditioner for CG in solving the system $\tilde{\Phi} \tilde{\beta} = \tilde{\mathbf{b}}$. In other words, we consider using the thresholding approximation on top of prior-preconditioning. Let $(\tau^2 \Lambda \mathbf{X}^\top \Omega \mathbf{X} \Lambda)_{(k)}$ denote a matrix obtained by thresholding the entries of $\tau^2 \Lambda \mathbf{X}^\top \Omega \mathbf{X} \Lambda$ to zero except for the $k \times k$ block corresponding to the k largest local scale parameters $\lambda_{(1)}, \dots, \lambda_{(k)}$. Then the thresholding approximation

$$\tilde{\Phi}_{(k)} = (\tau^2 \Lambda \mathbf{X}^\top \Omega \mathbf{X} \Lambda)_{(k)} + \mathbf{I}_p \quad (\text{S7})$$

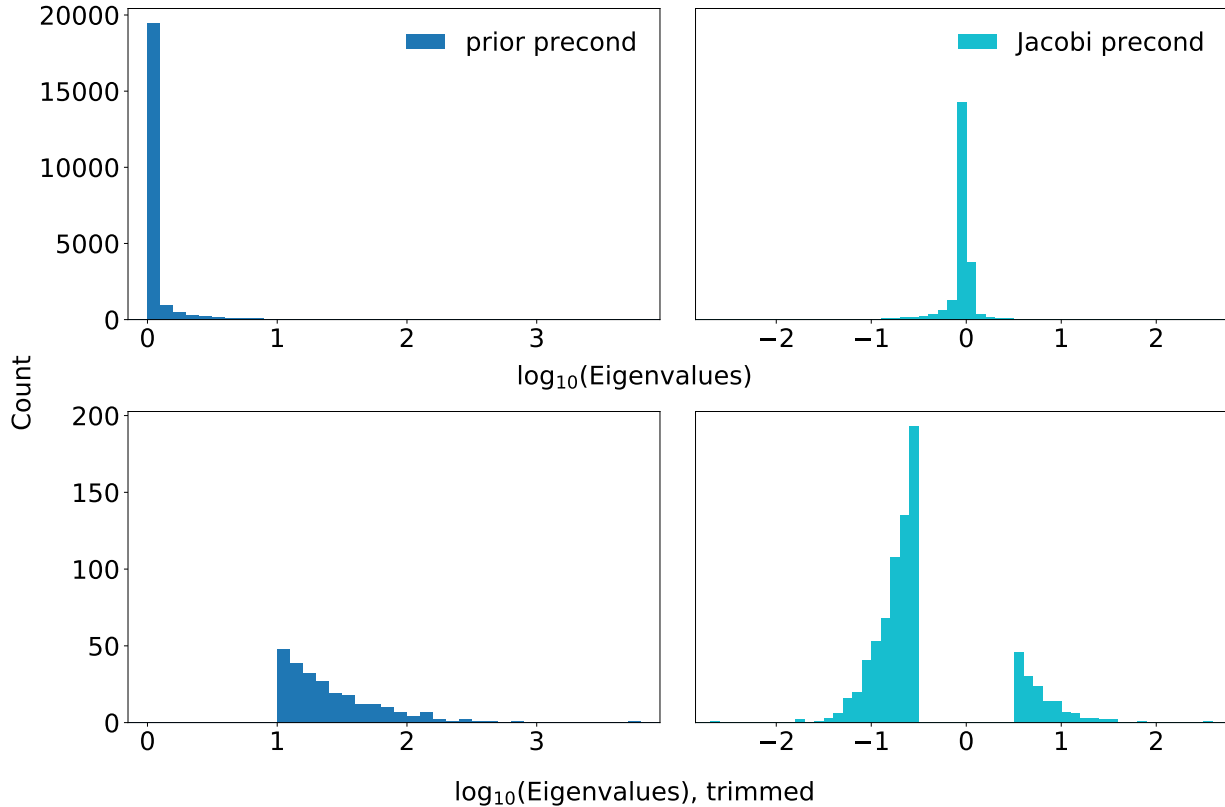


Figure S5: Histograms of the eigenvalues of the preconditioned matrices as in Figure 3.3. The only differences here are that 1) the preconditioned matrices are based on a posterior sample from the propensity score model (4.11) and 2) the trimmed version for the Jacobi preconditioner removes the eigenvalues in the range $[-0.5, 0.5]$ as this choice better demonstrates the tail behavior here.

is the identity perturbed by the $k \times k$ block along the diagonal. As such, using it as a preconditioner requires the one time cost of computing and factorizing the $k \times k$ block, which requires $O(k^2n + k^3)$ arithmetic operations. The quality of the approximation should improve as k increases but so does the computational cost. In particular, at some point the $O(k^2n + k^3)$ cost of preparing the thresholding preconditioner overwhelms the $O(np)$ cost of each CG iteration and becomes the computational bottleneck. When an adequate approximation requires such a large k , therefore, there is no benefit of using the thresholding approximation.

We use the example of Section 3.3 to study the effects of preconditioning the system

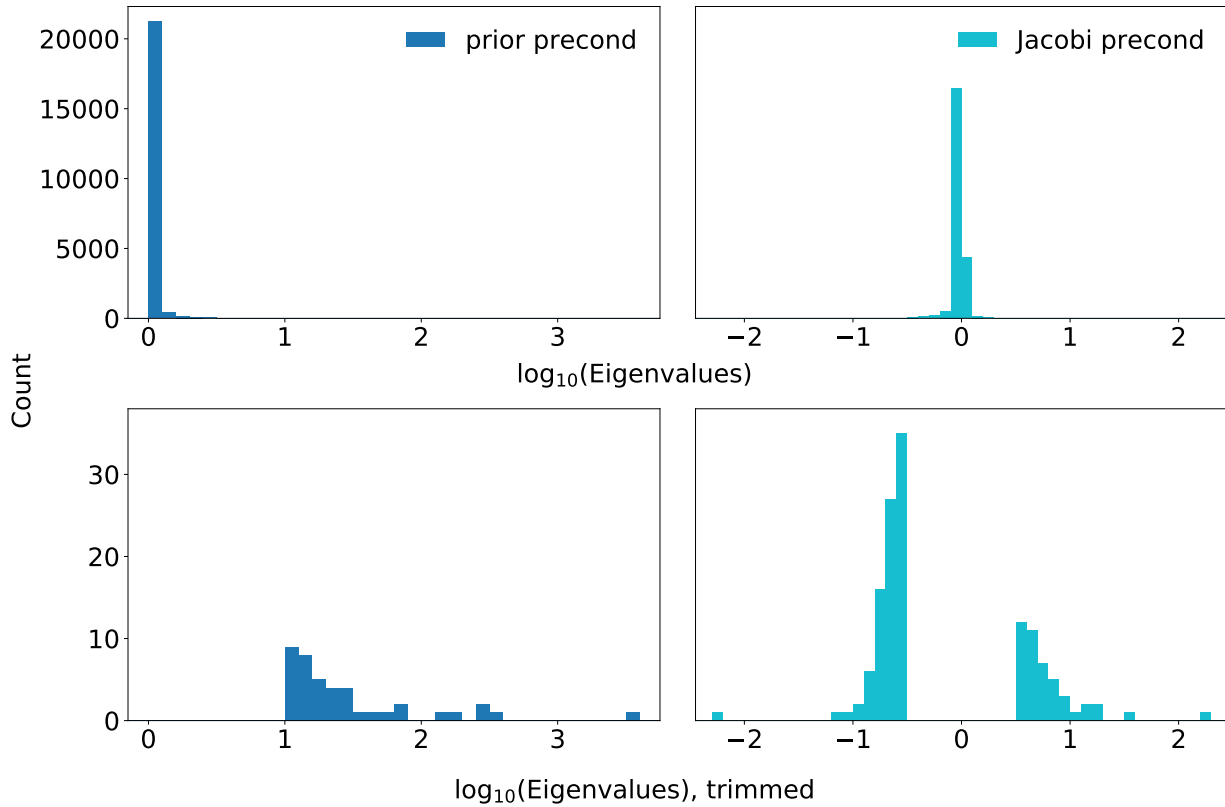


Figure S6: Histograms of the eigenvalues of the preconditioned matrices as in Figure 3.3. The only differences here are that 1) the preconditioned matrices are based on a posterior sample from the treatment effect model (4.12) and 2) the trimmed version for the Jacobi preconditioner removes the eigenvalues in the range $[-0.5, 0.5]$ as this choice better demonstrates the tail behavior here.

$\tilde{\Phi}\tilde{\beta} = \tilde{\mathbf{b}}$ with the thresholding approximation $\tilde{\Phi}_{(k)}$. As before, the CG sampler is applied to the distribution (1.2) arising from the simulated data with 10 signals out of $p = 10,000$ predictors. Figure S7 shows the results for $k = 1,000, 2,000,$ and $4,000$. The convergence rates of these preconditioned CG iterations are compared to that of the CG iterations applied to the prior-preconditioned system without any additional preconditioning. If a preconditioner is a good approximation of $\tilde{\Phi}$, the preconditioned CG should yield convergence in a very small number of iterations — for example, a perfect approximation would induce the convergence after one iteration. It is clear from Figure S7, however, that the thresholding approximation does more harm than good in terms of the CG convergence rate, especially when k is taken

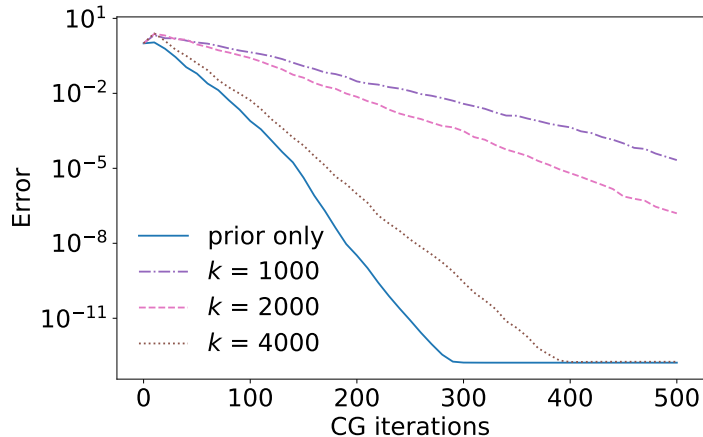


Figure S7: Plot of the CG approximation errors (with the same error metric as used in Figure 3.1) as a function of the number of CG iterations. The CG sampler here is applied to the conditional distribution of β arising from the simulated data example with 10 signals as described in Section 3. Each line corresponds to a different threshold level k for the approximation (S7). The blue line labeled ‘prior only’ corresponds to CG applied to the prior preconditioned system without any further preconditioner.

small relative to the size of $\tilde{\Phi}$. We can therefore conclude that the thresholding strategy yields a poor approximation except when k starts to become almost as large as p .

We repeated the same experiments on the thresholding approximation $\tilde{\Phi}_{(k)}$ using the other posterior distributions discussed in the manuscript. Across the experiments, no computational gain could be achieved by using the thresholding approximation as a preconditioner. More precisely, to yield a good enough approximation, the value of k had to be so large that preparing the preconditioner itself became a computational bottleneck.

S7 Proofs for Appendix B

Proposition B.1. As discussed in Section 2.2, the k -th CG iterate belongs to an affine space $\beta_0 + \mathcal{K}(\Phi, \mathbf{r}_0, k)$ with $\mathbf{r}_0 = \Phi\beta_0 - \mathbf{b} = \Phi(\beta_0 - \beta)$. An element β' of the affine space can be written as

$$\beta' = \beta_0 + \sum_{\ell=1}^k c_\ell \Phi^{\ell-1} \mathbf{r}_0 = \beta + (\beta_0 - \beta) + \sum_{\ell=1}^k c_\ell \Phi^\ell (\beta_0 - \beta)$$

for some c_1, \dots, c_k . In other words, for any β' in the affine space we can write

$$\beta' - \beta = Q_k(\Phi)(\beta_0 - \beta) \quad (\text{S8})$$

for some $Q_k \in \mathcal{P}_k$. Together with the optimality property (2.5) of the CG iterates, the representation (S8) implies

$$\|\beta_k - \beta\|_{\Phi} = \|R_k(\Phi)(\beta_0 - \beta)\|_{\Phi} = \min_{\beta' \in \beta_0 + \mathcal{K}(\Phi, r_0, k)} \|\beta' - \beta\|_{\Phi}. \quad \square$$

Theorem B.2. Let $\mathbf{v}_1, \dots, \mathbf{v}_p$ be the unit eigenvectors of Φ associated with the eigenvalues ν_1, \dots, ν_p . By the spectral theorem for normal matrices (Section 2.5 of Horn & Johnson (2012)), the unit eigenvectors form an orthonormal basis. In particular, we can write $\beta_0 - \beta = \sum_{j=1}^p c_j \mathbf{v}_j$ for $c_j = \langle \beta_0 - \beta, \mathbf{v}_j \rangle$. Observe that, for any $Q_k \in \mathcal{P}_k$,

$$\Phi^{1/2} Q_k(\Phi)(\beta_0 - \beta) = \sum_{j=1}^p c_j \Phi^{1/2} Q_k(\Phi) \mathbf{v}_j = \sum_{j=1}^p c_j \nu_j^{1/2} Q_k(\nu_j) \mathbf{v}_j.$$

Together with (B.15), the above equality yields

$$\|\beta_k - \beta\|_{\Phi}^2 \leq \sum_{j=1}^p c_j^2 \nu_j Q_k(\nu_j)^2 \leq \max_{j=1, \dots, p} Q_k(\nu_j)^2 \left(\sum_{j=1}^p c_j^2 \nu_j \right). \quad (\text{S9})$$

The result (B.16) follows from the above inequality since $\|\beta_0 - \beta\|_{\Phi}^2 = \sum_{j=1}^p c_j^2 \nu_j$.

The sharpness of the upper bound is proven by explicitly constructing an initial vector that achieves the bound; see Greenbaum (1979). \square

Theorem B.3. We can construct a shifted and scaled Chebyshev polynomial $P_k \in \mathcal{P}_k$ such that $|P_k(\nu)|$ is bounded by the right-hand side of (B.17) over the interval $[\nu_{\min}, \nu_{\max}]$. See Saad (2011) for further details. \square

Theorem B.4. Let Q_k^* denote the minimizer of $\max_{j=r+1, \dots, p} |Q_k(\nu_j)|$ over \mathcal{P}_k and define

$$Q'_{r+k}(\nu) = Q_k^*(\nu) \prod_{i=1}^r \left(\frac{\nu_i - \nu}{\nu_i} \right).$$

Then Q'_{r+k} satisfies $Q'_{r+k}(\nu_j) = 0$ for $j = 1, \dots, r$ and $Q'_{r+k}(\nu_j) \leq Q_k^*(\nu_j)$ for $j = r+1, \dots, p$.

In particular, Q'_{r+k} satisfies

$$\max_{j=1, \dots, p} |Q'_{r+k}(\nu_j)| \leq \max_{j=r+1, \dots, p} |Q_k^*(\nu_j)| = \min_{Q_k \in \mathcal{P}_k} \max_{j=r+1, \dots, p} |Q_k(\nu_j)|,$$

where the equality holds as we chose Q_k^* to be the minimizer. From the above inequality, it follows that

$$\min_{Q_{r+k} \in \mathcal{P}_{r+k}} \max_{j=1, \dots, p} |Q_{r+k}(\nu_j)| \leq \max_{j=1, \dots, p} |Q'_{r+k}(\nu_j)| \leq \min_{Q_k \in \mathcal{P}_k} \max_{j=r+1, \dots, p} |Q_k(\nu_j)|. \quad (\text{S10})$$

Since the maximum taken over an interval $[\nu_p, \nu_{r+1}]$ is larger than that over its subset, (S10) implies

$$\min_{Q_{r+k} \in \mathcal{P}_{r+k}} \max_{j=1, \dots, p} |Q_{r+k}(\nu_j)| \leq \min_{Q_k \in \mathcal{P}_k} \max_{\nu \in [\nu_p, \nu_{r+1}]} |Q_k(\nu)|. \quad (\text{S11})$$

The desired inequality (B.18) follows by bounding the right-hand side of (S11) via Theorem B.3. \square

Theorem B.5. We first prove the bound (B.19) for $C_{k,r,s}$ as defined in (S12) below. Let R_k be the optimal CG polynomial at the k -th iteration as defined in B.14. Since $R_k(0) = 1$, the polynomial $R_k(\nu)$ can be expressed in terms of its roots $\widehat{\nu}_1^{(k)}, \dots, \widehat{\nu}_k^{(k)}$ as

$$R_k(\nu) = \prod_{i=1}^k \left(\frac{\widehat{\nu}_i^{(k)} - \nu}{\widehat{\nu}_i^{(k)}} \right).$$

Now consider $Q_k \in \mathcal{P}_k$ such that

$$Q_k(\nu) = \prod_{i=1}^r \left(\frac{\nu_i - \nu}{\nu_i} \right) \prod_{i=0}^{s-1} \left(\frac{\nu_{p-i} - \nu}{\nu_{p-i}} \right) \prod_{i=r+1}^{k-s} \left(\frac{\widehat{\nu}_i^{(k)} - \nu}{\widehat{\nu}_i^{(k)}} \right)$$

and define

$$C_{k,r,s} = \max_{j=r+1, \dots, p-s} Q_k(\nu_j) / R_k(\nu_j). \quad (\text{S12})$$

As in the proof of Theorem B.2, write $\beta_0 - \beta = \sum_{j=1}^p c_j \mathbf{v}_j$ so that $\beta_k - \beta = \sum_{j=1}^p c_j R_k(\nu_j) \mathbf{v}_j$.

Let β'_k be a modification of β_k such that

$$\beta'_k - \beta = \sum_{j=r+1}^{p-s} c_j R_k(\nu_j) \mathbf{v}_j. \quad (\text{S13})$$

Choose $R'_\ell \in \mathcal{P}_\ell$ to be a minimizer of $\|Q_\ell(\Phi)(\beta'_k - \beta)\|_\Phi$ over $Q_\ell \in \mathcal{P}_\ell$ or, equivalently, the optimal CG polynomial (B.14) at the ℓ -th iteration when the initial vector is taken to be β'_k . Since $\beta_{k+\ell}$ minimizes the Φ -norm over the $(k+\ell)$ -th polynomial of degree by Proposition B.1, we have

$$\|\beta_{k+\ell} - \beta\|_\Phi \leq \|R'_\ell(\Phi)Q_k(\Phi)(\beta_0 - \beta)\|_\Phi. \quad (\text{S14})$$

We will now show that the right-hand side of (S14) is bounded above by that of (B.19). By our definition of β'_k and $C_{k,r,s}$ in (S13) and (S12), we have

$$\begin{aligned} \|R'_\ell(\Phi)Q_k(\Phi)(\beta_0 - \beta)\|_{\Phi}^2 &= \sum_{j=r+1}^{p-s} \nu_j c_j^2 R'_\ell(\nu_j)^2 Q_k(\nu_j)^2 \\ &\leq C_{k,r,s}^2 \sum_{j=r+1}^{p-s} \nu_j c_j^2 R'_\ell(\nu_j)^2 R_k(\nu_j)^2 \\ &= C_{k,r,s}^2 \|R'_\ell(\Phi)(\beta'_k - \beta)\|_{\Phi}^2. \end{aligned}$$

Noting that $\|\beta'_k - \beta\|_{\Phi} \leq \|\beta_k - \beta\|_{\Phi}$, we obtain

$$\|R'_\ell(\Phi)Q_k(\Phi)(\beta_0 - \beta)\|_{\Phi} \leq C_{k,r,s} \frac{\|R'_\ell(\Phi)(\beta'_k - \beta)\|_{\Phi}}{\|\beta'_k - \beta\|_{\Phi}} \|\beta_k - \beta\|_{\Phi}. \quad (\text{S15})$$

By our choice of R'_ℓ , the vector $R'_\ell(\Phi)(\beta'_k - \beta)$ coincides with the residual of the ℓ -th CG iterate starting from the initial vector β'_k . Therefore, by Lemma S7.1 combined with Theorem B.3, we have

$$\frac{\|R'_\ell(\Phi)(\beta'_k - \beta)\|_{\Phi}}{\|\beta'_k - \beta\|_{\Phi}} \leq 2 \left(\frac{\sqrt{\nu_{r+1}/\nu_{p-s}} - 1}{\sqrt{\nu_{r+1}/\nu_{p-s}} + 1} \right)^\ell. \quad (\text{S16})$$

The claimed inequality (B.19) now follows from (S14), (S15), and (S16).

Now we turn to proving the claimed property of $C_{k,r,s}$. Note that

$$\frac{Q_k(\nu)}{R_k(\nu)} = \prod_{i=1}^r \frac{\widehat{\nu}_i^{(k)}}{\nu_i} \left(\frac{\nu_i - \nu}{\widehat{\nu}_i^{(k)} - \nu} \right) \prod_{i=0}^{s-1} \frac{\widehat{\nu}_{k-i}^{(k)}}{\nu_{p-i}} \left(\frac{\nu_{p-i} - \nu}{\widehat{\nu}_{k-i}^{(k)} - \nu} \right).$$

The rest of the proof focuses on the case $r = 1$ and $s = 0$ for clarity's sake; the proof remains essentially identical in the general case except for extra notational clutters. Under this case, we have

$$\max_{j=2, \dots, p} \left| \frac{Q_k(\nu_j)}{R_k(\nu_j)} \right| = \frac{\widehat{\nu}_1^{(k)}}{\nu_1} \max_{j=2, \dots, p} \left| \frac{\nu_1 - \nu_j}{\widehat{\nu}_1^{(k)} - \nu_j} \right| = \frac{\widehat{\nu}_1^{(k)}}{\nu_1} \max_{j=2, \dots, p} \left| 1 - \frac{\widehat{\nu}_1^{(k)} - \nu_1}{\nu_j - \nu_1} \right|^{-1}.$$

Provided $|\widehat{\nu}_1^{(k)} - \nu_1| = \min_{j=1, \dots, p} |\widehat{\nu}_1^{(k)} - \nu_j|$, the above inequality simplifies to

$$\max_{j=2, \dots, p} \left| \frac{Q_k(\nu_j)}{R_k(\nu_j)} \right| = \frac{\widehat{\nu}_1^{(k)}}{\nu_1} \left| 1 - \frac{\widehat{\nu}_1^{(k)} - \nu_1}{\nu_2 - \nu_1} \right|^{-1}.$$

So we have $C_{k,r,s} \rightarrow 1$ as $\widehat{\nu}_1^{(k)} \rightarrow \nu_1$ in the case $r = 1$ and $s = 0$. \square

Lemma S7.1. Let (ν_j, \mathbf{v}_j) for $j = 1, \dots, p$ denote the eigenvalue and eigenvector pairs of Φ . If the initial vector β_0 satisfies $\langle \beta_0 - \beta, \mathbf{v}_j \rangle = 0$ for $j \in J \subset \{1, \dots, p\}$, then the bound (B.16) holds over the set $\{1, \dots, p\} \setminus J$ i.e.

$$\frac{\|\beta_k - \beta\|_{\Phi}}{\|\beta_0 - \beta\|_{\Phi}} \leq \min_{Q_k \in \mathcal{P}_k} \max_{j \notin J} |Q_k(\nu_j)|.$$

Proof. The proof is identical to that of Theorem B.2 except that we can replace the bound (S9) with

$$\|\beta_k - \beta\|_{\Phi}^2 \leq \sum_{j \notin J} c_j^2 \nu_j Q_k(\nu_j)^2 \leq \max_{j \notin J} Q_k(\nu_j)^2 \left(\sum_{j \notin J} c_j^2 \nu_j \right)$$

since $c_j = 0$ for $j \in J$ by assumption. □

References for Supplement

- Azad, A., Ballard, G., Buluc, A., Demmel, J., Grigori, L., Schwartz, O., Toledo, S. & Williams, S. (2016), ‘Exploiting multiple levels of parallelism in sparse matrix-matrix multiplication’, *SIAM Journal on Scientific Computing* **38**(6), C624–C651.
- Bank, R. E. & Douglas, C. C. (1993), ‘Sparse matrix multiplication package (smmp)’, *Advances in Computational Mathematics* **1**(1), 127–137.
- Davis, T. A. (2011), ‘Algorithm 915, SuiteSparseQR: Multifrontal multithreaded rank-revealing sparse QR factorization’, *ACM Transactions on Mathematical Software (TOMS)* **38**(1), 8.
- Dongarra, J., Heroux, M. A. & Luszczek, P. (2016), ‘High-performance conjugate-gradient benchmark: A new metric for ranking high-performance computing systems’, *The International Journal of High Performance Computing Applications* **30**(1), 3–10.
- Duff, I. S., Erisman, A. M. & Reid, J. K. (2017), *Direct methods for sparse matrices*, Oxford University Press.
- Duff, I. S., Heroux, M. A. & Pozo, R. (2002), ‘An overview of the sparse basic linear algebra subprograms: The new standard from the BLAS technical forum’, *ACM Transactions on Mathematical Software (TOMS)* **28**(2), 239–267.

- Matam, K., Indarapu, S. R. K. B. & Kothapalli, K. (2012), Sparse matrix-matrix multiplication on modern architectures, *in* ‘19th International Conference on High Performance Computing (HiPC)’, IEEE, pp. 1–10.
- Park, T. & Casella, G. (2008), ‘The Bayesian Lasso’, *Journal of the American Statistical Association* **103**(482), 681–686.
- Rue, H. & Held, L. (2005), *Gaussian Markov random fields: theory and applications*, CRC press.
- Saad, Y. (2011), *Numerical Methods for Large Eigenvalue Problems: Revised Edition*, Classics in Applied Mathematics, Society for Industrial and Applied Mathematics.
- Zucknick, M., Saadati, M. & Benner, A. (2015), ‘Nonidentical twins: comparison of frequentist and Bayesian lasso for Cox models’, *Biometrical Journal* **57**(6), 959–981.